AD-A113 612 VIRGINIA UNIV CHARLOTTESVILLE DEPT OF MECHANICAL AND--ETC F/G 21/5
THE SCHLADITZ FUEL INJECTOR: AN INITIAL PERFORMANCE EVALUATION --ETC(U)
MAR 82 G B MATTHEWS, J E SCOTT, K A HARVEY N00014-77-C-0564
UNCLASSIFIED UVA/525335/MAE78/101R NL

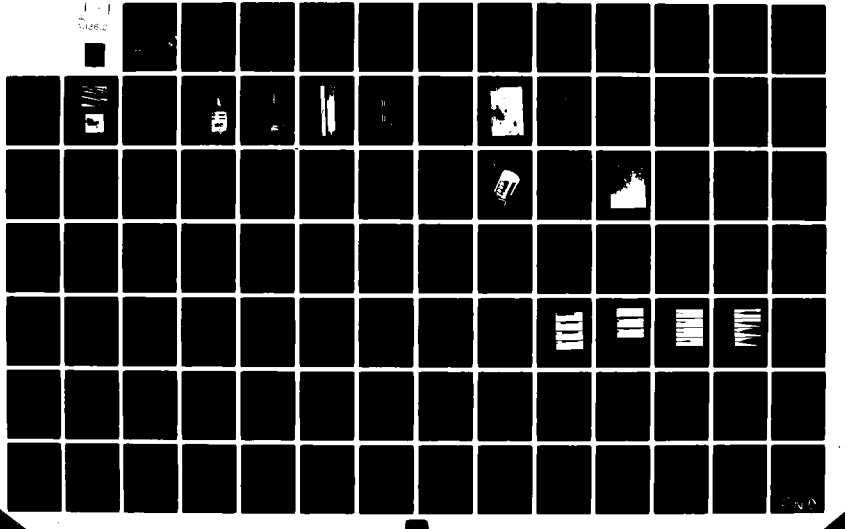

AD A113612

DTIC FILE COPY

A Report

THE SCHLADITZ FUEL INJECTOR: AN INITIAL PERFORMANCE EVALUATION WITHOUT BURNING

Submitted to:

Power Programs (Code 473)
Office of Naval Research
800 N. Quincy Street
Arlington, VA 22217

Submitted by:

G. B. Matthews
Professor

J. E. Scott
Professor

K. A. Havey, Jr.
Graduate Research Assistant

J. Z. Colt, Jr.
Graduate Research Assistant

Report No. UVA/525335/MAE78/101R

February 1979

Revised March 1982

DTIC ELECTE APR 20 1982 H

SCHOOL OF ENGINEERING AND APPLIED SCIENCE

DEPARTMENT OF MECHANICAL AND AEROSPACE ENGINEERING

UNIVERSITY OF VIRGINIA
CHARLOTTESVILLE, VIRGINIA 22901

DISTRIBUTION STATEMENT A
Approved for public release;
Distribution Unlimited

82 04 19 148

(12)

A Report

THE SCHLADITZ FUEL INJECTOR: AN INITIAL PERFORMANCE EVALUATION WITHOUT BURNING

Submitted to:

Power Programs (Code 473)
Office of Naval Research
800 N. Quincy Street
Arlington, VA 22217

Submitted by:

G. B. Matthews
Professor

J. E. Scott
Professor

K. A. Havey, Jr.
Graduate Research Assistant

J. Z. Colt, Jr.
Graduate Research Assistant

Department of Mechanical and Aerospace Engineering
RESEARCH LABORATORIES FOR THE ENGINEERING SCIENCES
SCHOOL OF ENGINEERING AND APPLIED SCIENCE
UNIVERSITY OF VIRGINIA
CHARLOTTESVILLE, VIRGINIA

Report No. UVA/525335/MAE78/101
February 1979

Copy No. 24
(Revised March 1982)

SECURITY CLASSIFICATION OF THIS PAGE (When Data Entered)

REPORT DOCUMENTATION PAGE	READ INSTRUCTIONS BEFORE COMPLETING FORM
1. REPORT NUMBER	2. GOVT ACCESSION NO. AD-A113 612 / 3. RECIPIENT'S CATALOG NUMBER
4. TITLE (and Subtitle) "The Schladitz Fuel Injector: An Initial Performance Evaluation Without Burning"	5. TYPE OF REPORT & PERIOD COVERED Final Report 09/01/77 - 02/28/79
	6. PERFORMING ORG. REPORT NUMBER UVA/525335/MAE78/101R
7. AUTHOR(s) G. B. Matthews, K. A. Havey, Jr., J. E. Scott, J. Z. Colt, Jr.	8. CONTRACT OR GRANT NUMBER(s) N00014-77-C-0564
9. PERFORMING ORGANIZATION NAME AND ADDRESS Department of Mechanical Engineering, University of Virginia, Thornton Hall, Charlottesville, VA 22901	10. PROGRAM ELEMENT, PROJECT, TASK AREA & WORK UNIT NUMBERS
11. CONTROLLING OFFICE NAME AND ADDRESS James R. Patton, Jr., Power Program, Department of the Navy, ONR, Arlington, VA 22217	12. REPORT DATE March 1982
	13. NUMBER OF PAGES 89
14. MONITORING AGENCY NAME & ADDRESS (if different from Controlling Office)	15. SECURITY CLASS. (of this report) Unclassified
	15a. DECLASSIFICATION/DOWNGRADING SCHEDULE NA

16. DISTRIBUTION STATEMENT (of this Report)

Approved for public release; distribution unlimited.

17. DISTRIBUTION STATEMENT (of the abstract entered in Block 20, if different from Report)

NA

18. SUPPLEMENTARY NOTES

The findings in this report are not to be construed as an official Department of the Navy position, unless so designated by other authorized documents.

19. KEY WORDS (Continue on reverse side if necessary and identify by block number)

combustion
fuel injection
atomization
particle size determination

20. ABSTRACT (Continue on reverse side if necessary and identify by block number)

Past tests of the Schladitz Fuel Injector (SFI), a network of electrically-heated, extremely-thin metal whiskers, have shown that very fine fuel droplet sprays are formed leading to substantial improvements in combustion efficiency. Evaluation of this performance potential, however, requires thorough investigation of the flow rate/pressure drop/heating rate influences on spray quality and droplet size distribution. Such tests were performed on two SFI geometries with steady flows of Jet-A fuel.

DD FORM 1 JAN 73 1473 EDITION OF 1 NOV 65 IS OBSOLETE

Unclassified
SECURITY CLASSIFICATION OF THIS PAGE (When Data Entered)

20. ABSTRACT (continued)

When these flows were discharged directly to the atmosphere, pressure drop reached a minimum at heating rates of 280 J/cc. At this point, spray quality improved noticeably, showing substantial fog or mist production, which became complete mist as the heating rate approached three-fourths the Jet-A enthalpy of vaporization. Similar tests of SFI flows exhausting through conventional spray nozzles showed appreciable improvement in spray quality, producing 50% or more mist at heating rates about one-third less than those required in the absence of nozzles. This improvement was essentially independent of the type nozzle employed, and all nozzle pressure drops were much less than those of the SFI.

Droplet size investigations included examination of spray samples on soot-coated slides and observations of laser light absorption. Both techniques indicated the presence of extremely fine droplets, of order 10 μm diameter or less, in the SFI-produced mists; and both supported the previous spray quality determinations, showing a monotonic decrease in mean particle size with increasing heating-to-flowrate ratio. Precise droplet size distributions were not determined, but theoretical analyses indicated that mean size trends with heating were not sensitive to assumed distributions.

Further tests to evaluate trade-offs between heating rate and nozzle pressure drop in terms of spray quality are recommended.

Accession For
NTIS GRA&I ☒
DTIC TAB ☐
Unannounced ☐
Justification
By
Distribution/
Availability Codes
Dist | Avail and/or Special
A

DTIC COPY INSPECTED 2

ABSTRACT

Production of very small droplets in a fuel injection system is an effective means of improving combustion performance, as demonstrated in past tests of the Schladitz Fuel Injector (SFI), a device in which extremely thin metal whiskers are placed in the fuel flow passages in the presence of an electrical heating coil. Potential improvements from this injector include the realization of greater combustion efficiency, establishment of wider flammability limits, and reduction in noxious pollutant products.

However, a meaningful evaluation of the performance potential of the SFI requires more complete understanding of the atomization process with heat addition in the whisker environment. To this end, initial tests of the flow-rate-pressure drop relationship were conducted over a wide range of heating rates, with concurrent observations of spray quality, limited sampling of droplets, and preliminary droplet size determinations from optical scattering. Two different injector geometries were tested at a series of steady flow conditions with Gulf Jet-A fuel in a simple, gas-pressurized feed system.

The results of one series of tests in which the flows from both injectors were discharged directly into the atmosphere showed that the pressure drop across the injector decreased monotonically until a heating rate of approximately 280 J/cc had been reached, beyond which the drop increased with any further heating. At this same critical heating condition, a noticeable change in the spray quality began to be evident in the form of substantial portions of the flow appearing as fog or

mist. Further heat addition brought about dramatic improvement in the spray atomization, with essentially complete mist appearing at a heating rate approaching three-fourths of the average enthalpy of vaporization of Jet-A fuel at atmospheric pressure.

A different pressure environment was provided in a second series of tests in which the SFI exhaust was fed through one of two spray nozzles before discharging into room air. These nozzles exhibited quite modest pressure drops in the range of flows investigated, with the major drop still occurring across the SFI itself. However, the spray quality evidenced by both injector models was improved substantially over that achieved at the same heating rate in the absence of the exit nozzle. Stated alternatively, the presence of the downstream nozzle reduced the required heat addition rate by about one-third for formation of a spray having 50% or more mist content. It was further noted that this heating rate reduction was essentially independent of the type nozzle employed, i.e., swirling, spring-loaded pintle or simple solenoid-operated orifice, and of the pressure drop across the nozzle over a range of from one to four atmospheres.

A limited amount of supporting evidence of the presence of very small droplets in the heated flows was obtained from soot-coated slides exposed to the spray by a simple rotating slit device. Reduction in mean droplet replica size and an increasing fraction of small droplets in the spray were both observed in these slide samples as heating rate was increased.

A more objective means of determining the effect of different operating conditions on droplet size was developed utilizing laser light

scattering and absorbing properties of the spray. Simple physical arguments were combined with Mie theory to develop consistent evidence of relative changes in the mean size of the spray distribution as a function of heating rate-to-flowrate ratio and of nozzle pressure drop. Results of these tests reinforced the simpler soot slide observations, indicating a decreasing drop size with increasing heating rate and pressure drop. The relative size index thus obtained is shown to be an approximate upper limit to the actual dimensions of the fuel droplets.

Analysis of the injected fluid thermodynamic states on an enthalpy-temperature plot for Jet-A fuel suggests that the creation of a fine mist by the SFI in the absence of any downstream nozzle is accompanied by the formation of a measurable fraction of vapor within the injector, while a similar spray formed by the SFI-nozzle combination is essentially free from any vapor until the isenthalpic expansion occurs through the nozzle.

Further verification of the test results to date, with a more detailed evaluation of the trade-offs between heat additions and nozzle pressurization, is recommended for the future as a logical extension of the present work.

TABLE OF CONTENTS

LIST OF FIGURES

LIST OF FIGURES (continued)

LIST OF TABLES

SECTION 1

INTRODUCTION

The production of very small liquid fuel particles in a combustion injection system is highly desirable as a means of improving the vaporization of the fuel and, hence, the performance of the combustion system. When this process of subdivision of the bulk liquid fuel into smaller particles, usually called atomization, involves the production of very fine droplets (under 10 μm in diameter), the phenomenon is called nebulization. For spherical fuel particles, the vaporization rate per unit mass of fuel is proportional to the ratio of the surface area of the particle to its volume, that is, to the reciprocal of the particle diameter. Consequently, efficient nebulization and its resultant small particle sizes correspond to high vaporization rates and accompanying improvements in performance. In existing combustion systems such improvements could result in reduced specific fuel consumption and increased range of aircraft and ships. Alternatively, these improvements could enable the use of a lower grade, cheaper fuel of higher availability in a given combustion system without appreciable loss of performance when compared to current fuels.

Several years ago, Mr. Hermann Schladitz, of Munich, Germany, developed a device which nebulizes liquid fuel into a very fine mist in order to achieve cleaner and more complete combustion. The device, called a Schladitz Heat Exchanger, consists of a very large number of small polycrystalline whiskers sintered together to form a porous network or skeleton which is then surrounded by a heating element. The polycrystalline whiskers (with diameters in the range 0.3-20 μm and

length-to-diameter ratios in the range 10^3 - 10^4) are produced by the thermal decomposition of metal carbonyl vapors, e.g., Fe, Ni, Cr, in the presence of a magnetic field. (Study of the whisker production mechanism is under way currently at the University of Virginia under the sponsorship of the Metallurgy Branch of ONR). Whiskers produced in this manner have a large surface area (see Figure 1) and, since they are metal, can easily be heated to further prepare a liquid fuel passing through the whisker network for subsequent vaporization, mixing, and combustion. Used as a fuel injection scheme, the Schladitz Fuel Injector (SFI) is a kind of porous plug made of very small diameter, long metal whiskers. Liquid fuels forced under pressure through an SFI emerge as a very fine mist (see Figure 2), the degree of nebulization (or atomization) of a given fuel being governed primarily by the porosity, the type and size of whisker material, the amount of energy supplied as heat to the device (usually by ohmic heating), and the pressure drop imposed upon the discharge nozzle.

Qualitative experimental results on the performance of the device tend to indicate that it is an exceptionally good fuel atomizer and has the potential capability of providing substantial improvement over existing combustion systems using liquid fuels ranging from residual fuel oils to high grade jet fuel. The improved high quality of fuel atomization must certainly enhance the performance of a combustion system by increasing combustion efficiency, broadening flammability limits, and possibly improving the quality of combustion product emission. Any further development of the SFI, however, will be dependent upon a thorough understanding of the nature of the critical process of atomization with heat addition in the whisker environment.

Figure 1 Scanning Electron Micrograph of Schladitz Whiskers Showing Nodular Surface

Figure 2 Fuel Mist Produced by a Whisker Fuel Injector

SECTION II

DESCRIPTION OF APPARATUS

Two configurations of the Schladitz Fuel Injector have been studied in an attempt to evaluate the overall flowrate-pressure drop characteristics, heating requirements, and spray particle sizes. A two-section design (Figure 3) designated SFI #1, or the "Pancake" model, is a multiple-tube arrangement, not unlike an ordinary heat exchanger, wrapped with an electrical heating element. The "tubes" are actually a series of holes drilled in a solid block of steel. Each tube is filled with nickel whiskers, restricted in their axial movement by a screen placed at the downstream and of the solid block. Each of the two sections has individual fuel input and exit connections, a heating element, and 2 thermocouples. The heating elements are Nichrome wire insulated by a coating of magnesium oxide. The resistance of one such heating element is approximately 14 ohms. Two iron-constantan thermocouples are provided with each section: one near the discharge (thermocouple #1) and one imbedded in the heating coil (thermocouple #2). In the original configuration, both sections of SFI #1 were insulated as a unit by wrapping with a ceramic felt material.

The three-section design, SFI #2, provides only one flow path per section (Figure 4), a whisker-filled volume in the shape of a long annulus between two coaxial cylinders, with the outer cylinder encircled by the heating element. The resistances and material of the heating elements are similar to those used in SFI #1, as are the type and arrangement of the two thermocouples. Each section of SFI #2 is individually insulated with ceramic felt, and the whisker material is iron rather than nickel.

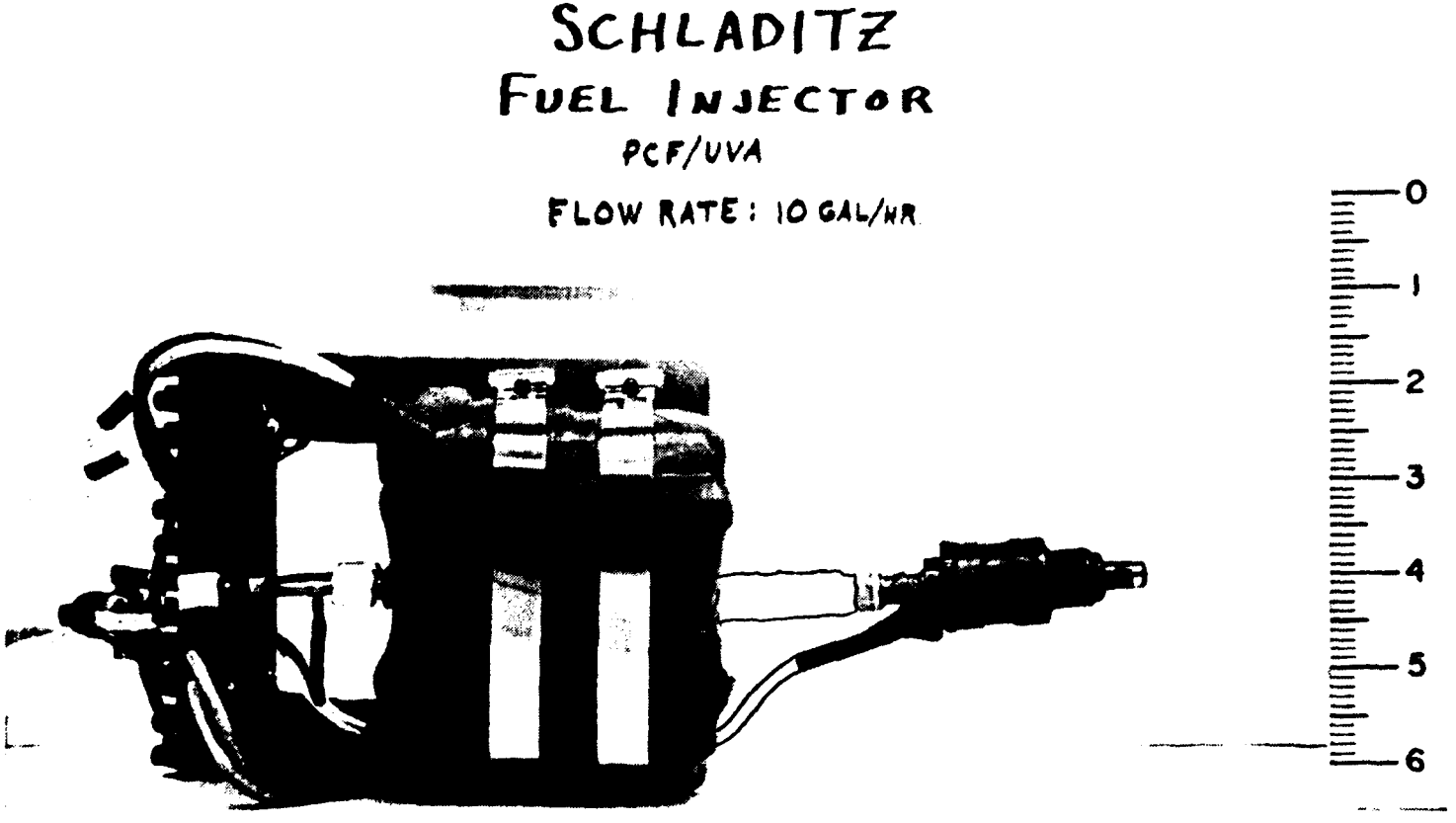

Figure 3a Photograph of SFI 1

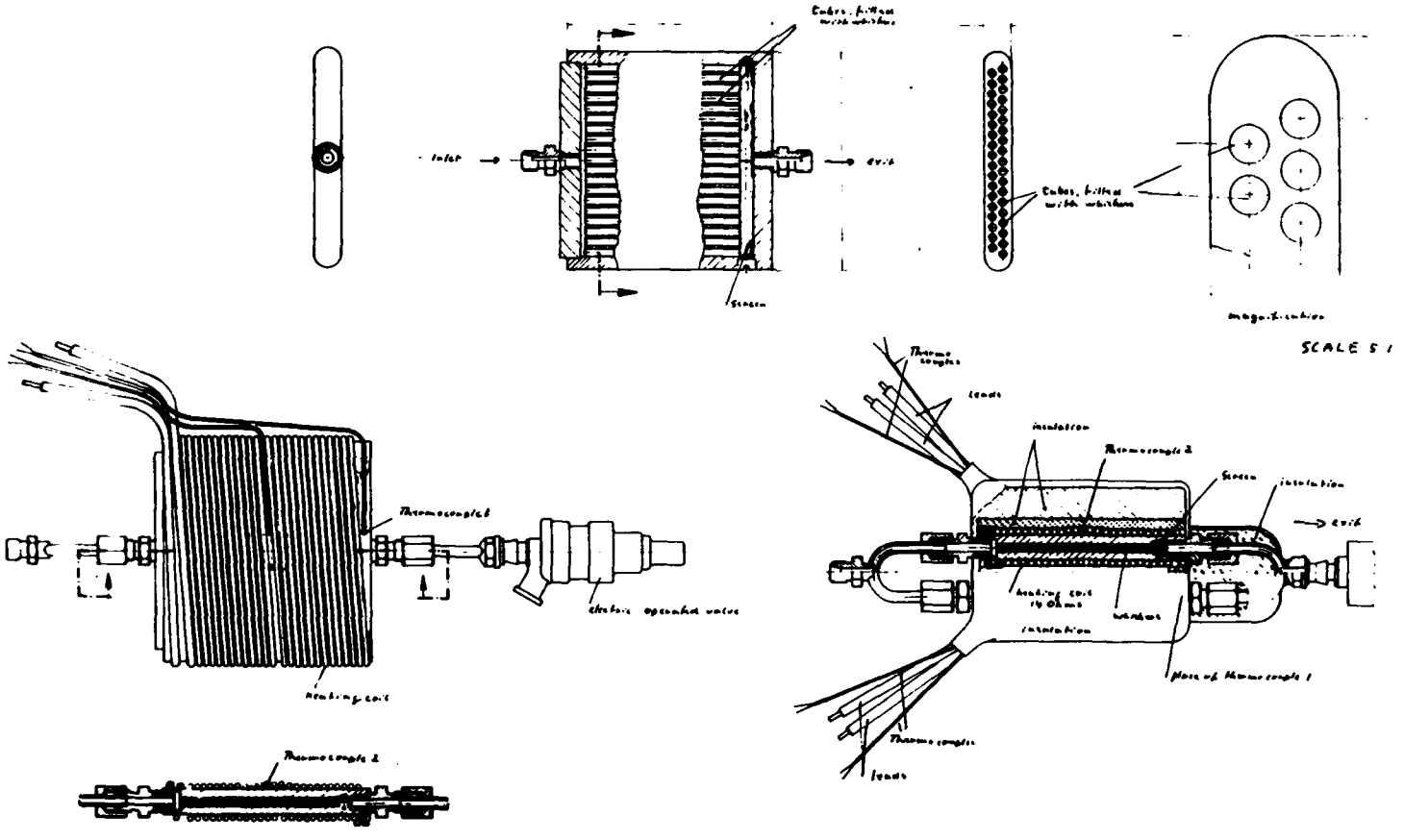

Figure 3b Schematic Diagram of SFI 1

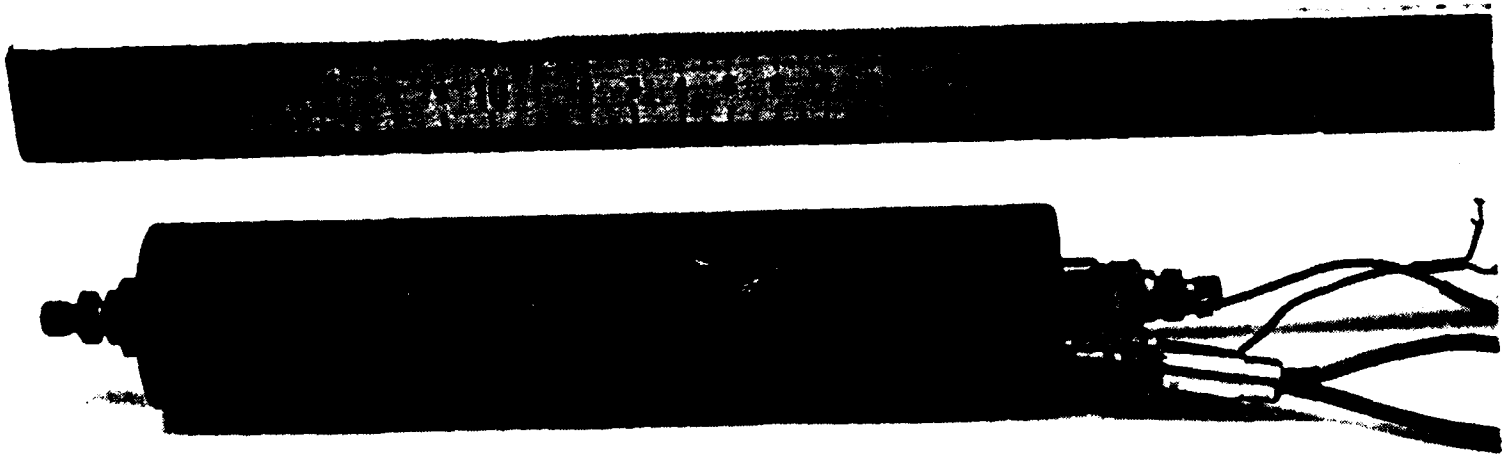

Figure 4a Photograph of SFI 2

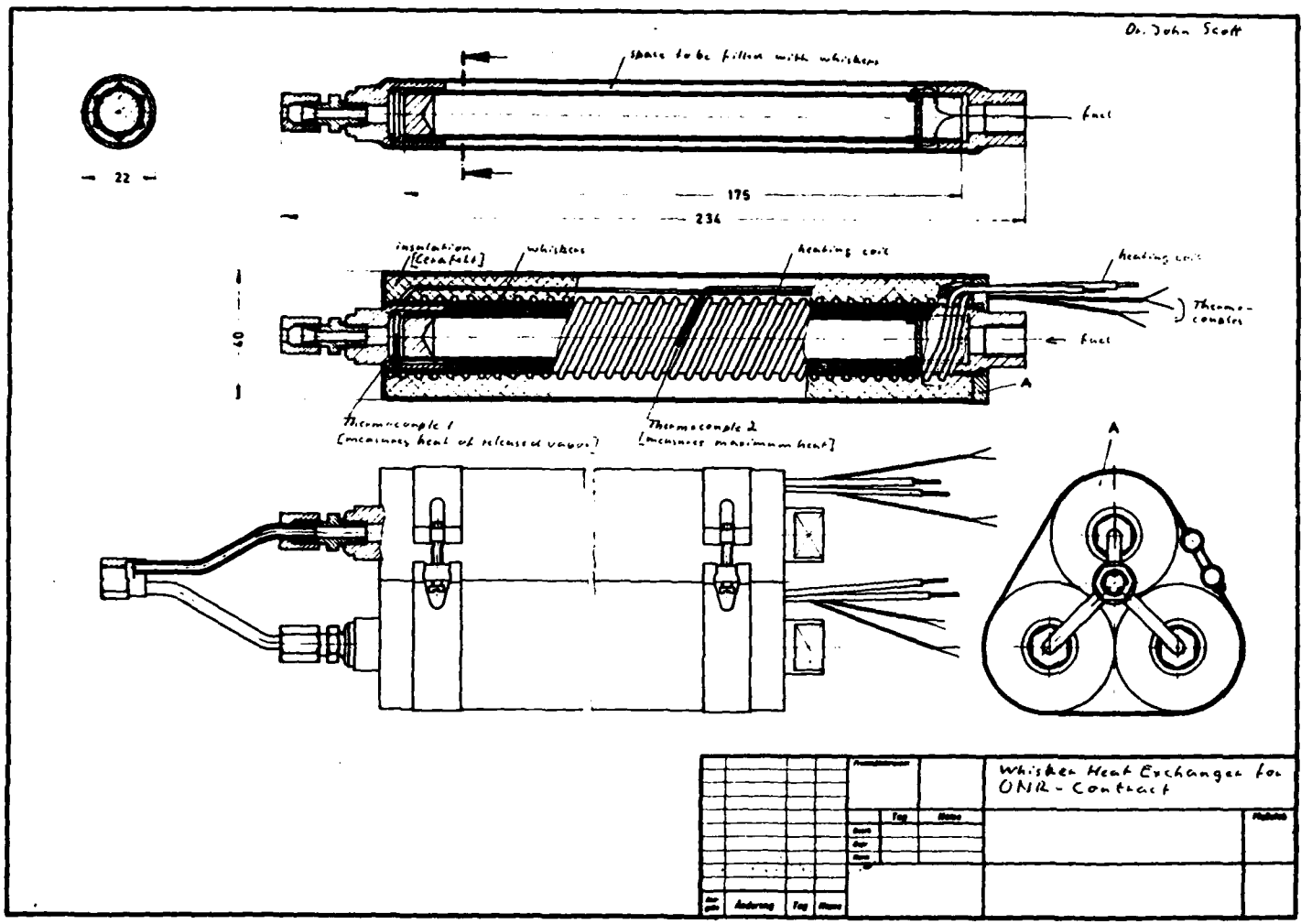

Figure 4b Schematic Diagram of SFI 2

On the downstream end of the injector, two different discharge nozzles were used at different times to provide a pressure drop after passage of the fluid through the whisker network. The first of these nozzles is an electrically-operated valve which displays very little tendency to produce spray or mist when operated without the whisker network. The pressure drop-flowrate relationship for this nozzle is essentially linear over the working range. As a second candidate configuration, a pressure-operated Bosch nozzle, designed for use in a passenger car fuel injection system, was used. This nozzle has a variable geometry because of its spring-loaded valve, and it exhibits an almost constant pressure drop over a wide range of flowrates. The nozzle is designed to produce a fuel spray independent of the presence of the whiskers upstream.

In all flow tests, fuel was supplied to the injector by a pressurized tank system consisting of a compressed gas bottle, a pressure regulator, a fuel reservoir, a filter, and a liquid flow control valve (Figure 5). Nitrogen from the gas bottle was regulated through a variable-pressure regulator and was used to pressurize the gas in the volume above the fuel level in the reservoir. Typical working pressures in the fuel reservoir, which has a volume of approximately 60.5 liters (16.0 gal.), range from 500 to 2000 KPa (64 - 300 psi), depending on the desired flowrate. Tank pressure was displayed on one scale of a Marsh Instruments "Duplex" (double-indicator) bourdon-tube gauge. Fuel leaves the reservoir under pressure through an exit positioned below the fluid level.

Figure 5a Photograph of SFI Testing System

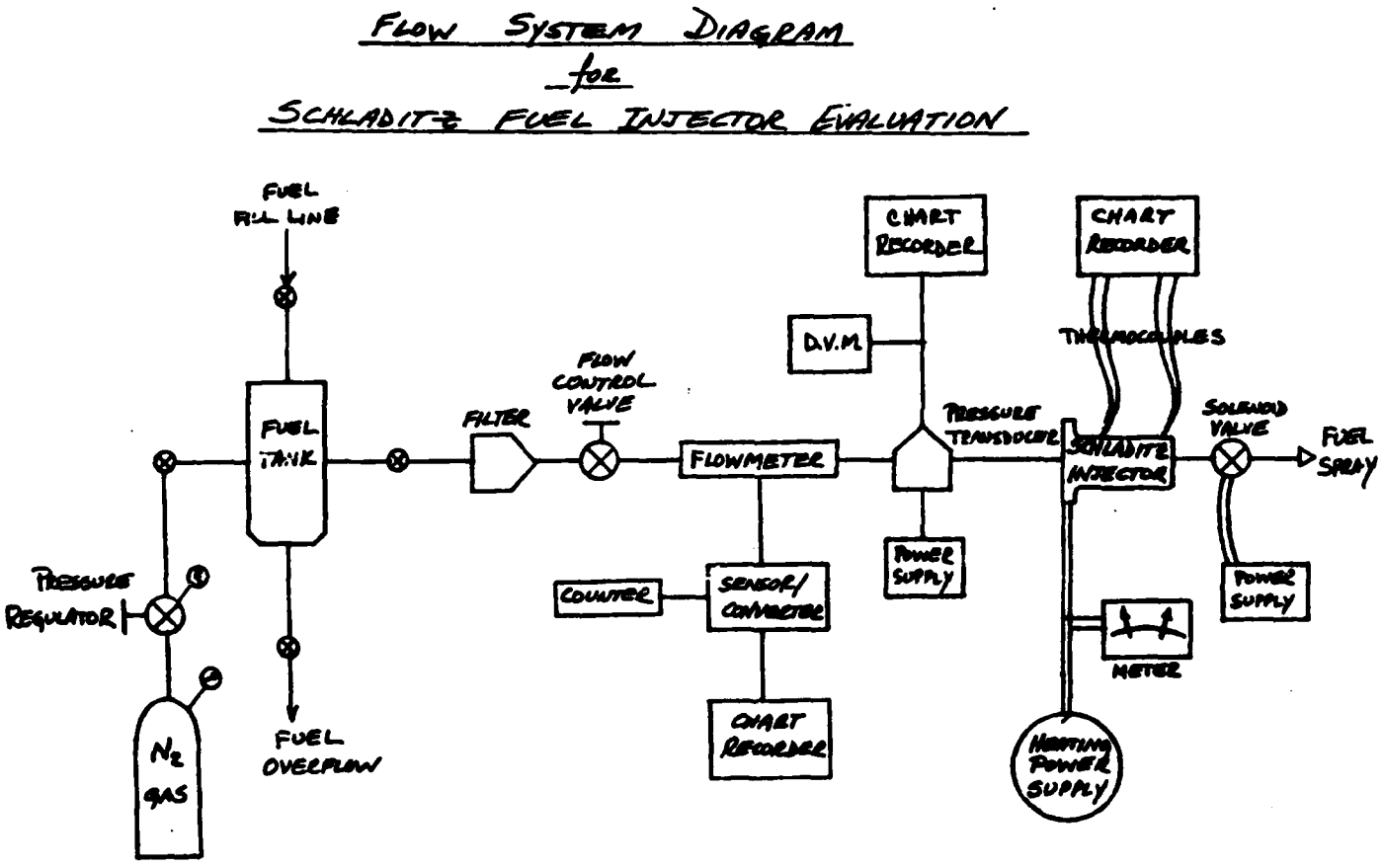

U.V.A./ONR CONTRACT N00014-77C-0564
16 FEBRUARY 1978

Figure 5b Schematic Diagram of
SFI Testing System

All liquid passing from the reservoir passes through a filter, which has a replaceable element made of sintered stainless steel. Rated pore sizes for different filter elements used ranged from 2 μm to 15 μm. The hand-operated fuel control valve served as the final flowrate control, providing fine adjustment.

The basic properties of the flow are monitored by three instruments: a "Bearingless" turbine flowmeter, a strain-gauge pressure transducer sensing injector inlet pressure, and a Heise bourdon-tube pressure gauge indicating injector exit pressure when this pressure is greater than atmospheric.

The Bearingless flow meter, in which the signal produced is a pulse of light converted to an electrical square wave, was calibrated over the range from 1.26 ml/sec to 200 ml/sec. The frequency of the square wave signal is proportional to the volumetric flow rate through the flow meter. A digital frequency counter was used to display this information. Calibration curves, plotting frequency as a function of volume flowrate, were generated by running both water and jet fuel A through the flow meter at a fixed frequency for a measured amount of time into a beaker of known empty weight. The mass of the filled beaker was measured on a balance, and the volume flowrate was calculated from the mass of fluid, the known density of the fluid at room temperature, and the elapsed time of the flow. The density of Jet-A was obtained from a plot of density and temperature supplied by Gulf Oil Corporation, the manufacturer, while the density of water used in the tests was taken to be 0.998 Kg/liter at 19^{o}C. Temperature was measured by a standard mercury-

in-glass thermometer. It should be noted that the flowmeter was originally placed downstream from the flow-control valve; but more consistent calibration results were obtained by placing it in the more nearly constant pressure region upstream from the valve, which then became its permanent location.

Fuel pressure at the inlet of the injector was monitored by the strain-gauge type pressure transducer (Viatran #103) and the other half of the "Duplex" gauge. This "Duplex" gauge was not used to acquire data, but simply as a visual indicator, giving a rough value of pressure and some indication of how the pressure was changing with time, with the strain-gauge transducer acting as the primary pressure monitor at the whisker network inlet. The electrical signal from the transducer was displayed on a Keithley #106B digital multimeter. Typical output voltages during a run ranged from 15 to 20 mv, corresponding to pressures of approximately 1000 KPa to 1300 KPa.

Since the pressure transducer was not located exactly at the inlet to the whisker network but was separated from it by a short length of copper tube, a correction factor was included in the data-reduction program to compensate for the pressure drop of the tubing. This correction factor is a function of flowrate and was found by measuring the pressure drop-flowrate characteristics of the tube with the whisker network detached. In this manner a more accurate value of the actual pressure existing at the input of the whisker network was established.

When the exit pressure from the whisker network was larger than one atmosphere (as is the case when a nozzle is used downstream), a bourdon-tube Heise gauge was connected to a fitting between the whisker package

and the nozzle. This Heise gauge is readable to 0.05 psi, having a range of 0-100 psi. Both the Viatran transducer and the Heise gauge were calibrated with a dead weight tester, with the pressure transducer calibration spanning a 0-300 psi range.

Thermocouple outputs were referenced to an ice point cold junction and displayed individually on the Keithley digital voltmeter by means of a switching network. A visual indication of temperature was provided by displaying the thermocouple outputs continuously on a multi-channel chart recorder. Using this chart recorder, it was easier to determine when the system had reached thermal equilibrium. The constant visual display also proved useful in detecting sudden transients in the fuel flow and malfunctions in the heating elements.

Electrical power for the heating elements, sometimes exceeding 1 KW per element, was obtained from a 208-volt, split-phase AC line, with voltage controlled by means of an autotransformer (Superior Electric Company "Powerstat"). The voltage across the heating elements was displayed continuously by a Westinghouse panel meter and a Non-Linear Systems, Inc. Series X3 digital voltmeter. The current was also displayed by a General Electric panel meter. The entire circuit was protected by a 20-ampere fuse in series with the input to the autotransformer.

Additional apparatus was assembled for optical investigation of droplet sizes in the heated sprays, for which tests the Schladitz fuel injector and its accompanying spray nozzle were mounted so as to discharge vertically downward into a plexiglas duct having a square cross

section of about 900 cm^2. This specialized test set-up, as shown schematically in Figure 5c, included a water-cooled Schladitz whisker network from which the condensed liquid fuel was collected for re-use. A vacuum blower was used to draw the droplets through the condenser, producing a net downward air velocity of approximately 1/3 meter/second. A Spectra-Physics 5 mw He-Ne laser (λ = 6328A) was used as a photon source, arranged to project a horizontal beam through the spray at a point approximately 40 cm downstream from the nozzle exit. A photomultiplier tube was placed opposite the laser to receive the beam, and a scale was mounted horizontally on the outside surface of the duct as a means of estimating the optical path length of the laser within the spray.

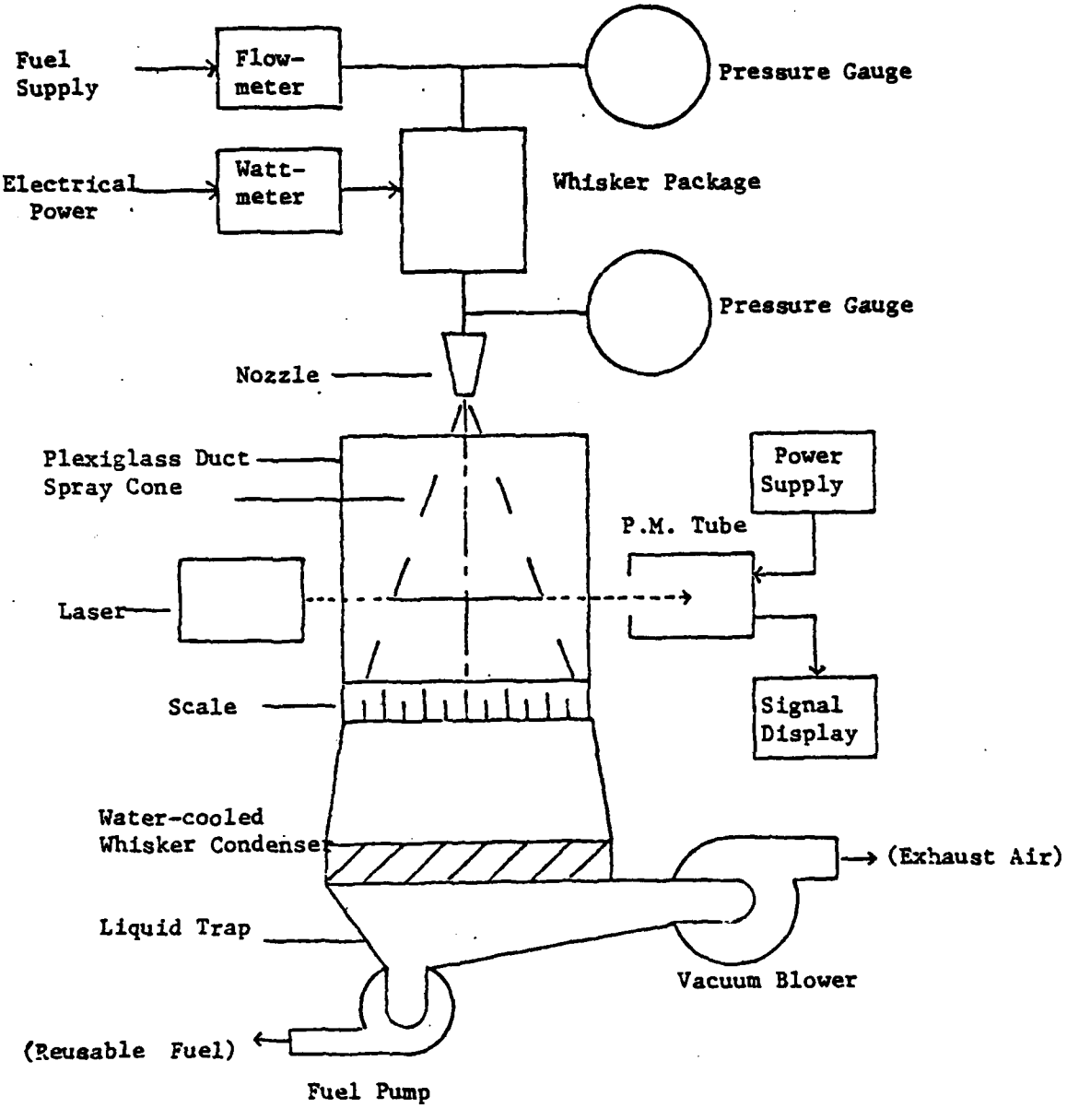

Figure 5c. Schematic Diagram of Droplet Measurement Apparatus

SECTION III

PROCEDURES

A number of different test procedures were used to determine the flow characteristics and performance of the SFI.

A. PRESSURE DROP MEASUREMENTS

Initial flowrate-pressure drop tests (SFI #1 with water) were carried out by simply setting the desired flowrate, using the flow control valve, and observing the flowrate indicator on the digital frequency counter, recording the measured (millivolt) reading from the pressure transducer after it reached equilibrium. No particular attention was paid to the time between readings, nor were any tests of flowrate changes with time made during the initial tests. Shortly thereafter, all tests were made with "time of reading" recorded for each data point taken. A steady increase with time of the pressure required to achieve a particular flowrate was discovered, and tests with water were suspended. Because of the concern for possible rust formations none of the elements of SFI #2 were used with water.

Acetone and dilute citric acid were alternately forced through SFI #1 (as per Professor Schladitz's recommendation) to remove suspected clogging material, and tests with Jet Fuel "A" were initiated. Cold Flow tests comparable to those previously made with water were carried out as follows: flowrate was set at a fixed value, and pressure readings were taken every 30 seconds (or 15.0 sec for some runs) for 3 minutes. During the three minute interval, the fluid exiting the system was collected in a beaker (of known mass) and weighed to calibrate the flowmeter for jet fuel. This procedure was repeated for 26 different

flowrates ranging from .593 cc/sec to 5.954 cc/sec. Above 5.954 cc/sec, total run times were reduced to 90 sec, with an interval between readings of 15 sec. Nine more flowrates were measured using this procedure, extending to a maximum volume flowrate of 13.7 cc/sec. The temperature of the collected fluid in the beaker was measured with a Brooklyn mercury-in-glass thermometer.

Heated flow tests without a pressure-drop nozzle downstream from the injector,were all made with a fixed flow, variable heating rate format. Pressure, flowrate, and electrical heating voltage and current values were recorded every 60 seconds. Temperature data from the thermocouples were displayed and recorded continuously on a stripchart recorder. Spot-checks of thermocouple readings were made with the digital voltmeter at irregular intervals during the test, to serve as calibration points on the chart.

At the beginning of the test, an initial flowrate was established, and conditions were allowed to stabilize before heat was added. After voltage was applied to the heating element, pressure and flowrate were allowed to adjust themselves, the pressure level being maintained roughly constant by the tank pressure regulator, with values recorded each minute. A given heating rate was maintained until the output from the thermocouples reached an essentially constant value, which condition usually was taken to be an indication of thermal equilibrium. Such equilibrium was achieved in a time interval of 6 minutes or less. Once thermal equilibrium had been reached, a spray "quality" evaluation was made, and a photograph was taken. Spray quality was estimated on the basis of what percent of the spray consisted of "mist", the fine, white,

cloudlike component. An approximate 10% "mist" spray received a rating of 1, and so on up to 100% "mist", which received a rating of 10. Thus rating = $\frac{\text{estimated \% mist}}{10}$. Occasional temperature measurements were made at the exit of the injector using one of the mercury-in-glas thermometers placed directly in the stream.

A cold flow test with a pressure-drop-producing nozzle downstream was made following the same format as pressure-drop-producing previous cold flow tests, except that values of flowrate and pressure were observed every 60 seconds for 1 hour, and no calibration of the flowmeter was carried out. Also, the pressure between the whisker package and the nozzle was observed on the Heise gauge and recorded each minute.

Heated tests, with downstream pressure drops, followed three different formats and included actual spray sampling. Initially, heated tests with a nozzle were carried out with the same procedure as the heated tests without a nozzle, except for observation of the additional pressure value resulting from the presence of the nozzle. This procedure duplication was carried out in order to compare the performance of the injector under similar conditions, both with and without a downstream pressure drop.

Since initial testing had demonstrated that heating rate and downstream pressure drop have a great influence on spray quality, tests were run with the downstream pressure fixed and the heating rate variable, as well as with heating rate fixed and the downstream pressure varying. In both of these test formats, adjustments were made to the "fixed" value to ensure that it would remain relatively constant during a test.

Adjustments to the nozzle pressure drop were made by simply adjusting the flowrate. The voltage necessary to achieve a particular heating rate, $\dot{Q}/\dot{V}$, was found by calculation, using the measured volume flowrate and measured value of the resistance of the heating element. Using both of the above techniques, either flowrate, and hence pressure drop, or heating rate could be adjusted independently of each other. As in previous heated tests, pressure, flowrate, voltage, and current data were recorded each minute. Gauge pressure at the inlet to the whisker package was monitored by the pressure transducer, and the pressure drop across the nozzle, discharging to atmosphere, was monitored by the Heise gauge as before.

B. SPRAY EVALUATION

The mean fuel spray droplet diameter and the distribution of particle sizes about this mean were chosen as the primary quantitative indices of injector performance to support the qualitative evidence obtained from visual and photographic observations. One attractive method for obtaining such size data involves the use of optical scattering techniques, particularly laser scattering, since measurements of very small (sub-micron) particles can be made by simply shining a light beam through the droplet cloud, observing the resultant disperson of the beam, and inferring the corresponding droplet distribution from well-established theory. This non-invasive experimental method eliminates any possible errors due to deformation of the droplets and their adjacent air flow field because of collisions with a solid collector or probe inserted in the stream. In addition, the use of optical scattering techniques minimizes the necessity for calibrating the measuring instrument against a standard particle-size sample.

However, the selection of the particular laser scattering-droplet size determination technique from the large number of such methods currently available requires prior knowledge of the specific range of sizes anticipated in the sample, each size range requiring slightly different procedures and theoretical relationships to make the technique valid.

Thus, in order to justify the use of any laser scattering technique, the existence of micron-size droplets in the spray must be established; and to select the optimum method, the approximate size distribution should also be known. To this end, a rapid, simple and convenient

particle sampling technique was sought. Straightforward techniques involving insertion of glass slides into the spray and subsequent microscopic examination of the surface of the slides were attempted. Plain glass slides were tried as well as those coated with various substances suggested in the literature (Refs. 4,6,7). Among the coatings investigated were talc, paraffin wax, glycerine, teflon, and soot from a kerosene flame. Of these, the teflon, wax, and talc coatings exhibited either a surface roughness or a grain size large enough to obscure the traces of captured particles. Although glycerine-coated slides showed a propensity for capturing small droplets, it was quite difficult to distinguish between these traces and those left in the glycerine coating by some other artifacts, such as room dust. A dry coating was therefore chosen, with carbon soot offering the best combination of grain size, ease of handling, and visible permanent record of each sample taken. Initial investigations of the spray patterns from both injectors were then conducted with soot-coated slides.

The soot coating was formed on the glass slides by passing them repeatedly through a smoky flame of kerosene oil, until the slide was completely coated and opaque. This yielded a coating with a thickness on the order of 50-100 μm. Thinner coatings were tried, albeit unsuccessfully in that replica profiles became very inconsistent, except for the smallest particle ranges. Impact sites smaller than 10 μm did not seem to be better defined in the thinner soot layer, so the thick coatings were retained. Each slide was numbered at one end, and this number was used as a guide to the orientation of the slide in its placement in the "sampler" and under the microscope. On the microscope stage, which was

equipped with a positioning device, slides were always placed with the number to the viewer's left, and the coordinates of each "sweep" were read on the positioner, which was readable to 0.1 mm along its x-and y-axes.

Initially, collection was accomplished by placing a card in the spray stream and passing a soot-covered slide across a slot cut in the card. This method was used for the first twenty-four slides made; but a number of slides taken prior to #25 were found to be totally saturated or to be nearly devoid of measurable particle impaction sites. In an effort to produce more consistent results, therefore, a shutter mechanism was constructed from two wooden disks and an open-ended steel "can" (see Figure 6). A slot was made in one disk, slightly smaller than the dimensions of a glass microscope slide. A "pie slice" (included angle of 30°) was cut out of the remaining disk. By rotating the second disk directly in front of the "slotted" disk, a slide placed behind the slot could be exposed to the stream of particles for varying amounts of time, depending upon the angular velocity of the rotating disk. The back of the slide was protected by the "can" which fit the disk tightly.

The rotating disk was turned manually, with a crank. An average speed for the disk was approximately 6 rad/sec, producing an effective average exposure time of .087 sec. For very fine sprays (or sprays that would qualitatively be rated at "90% mist"), some samples were taken at a slower shutter speed to facilitate the collection of smaller particles which lose linear momentum faster than larger particles, thereby

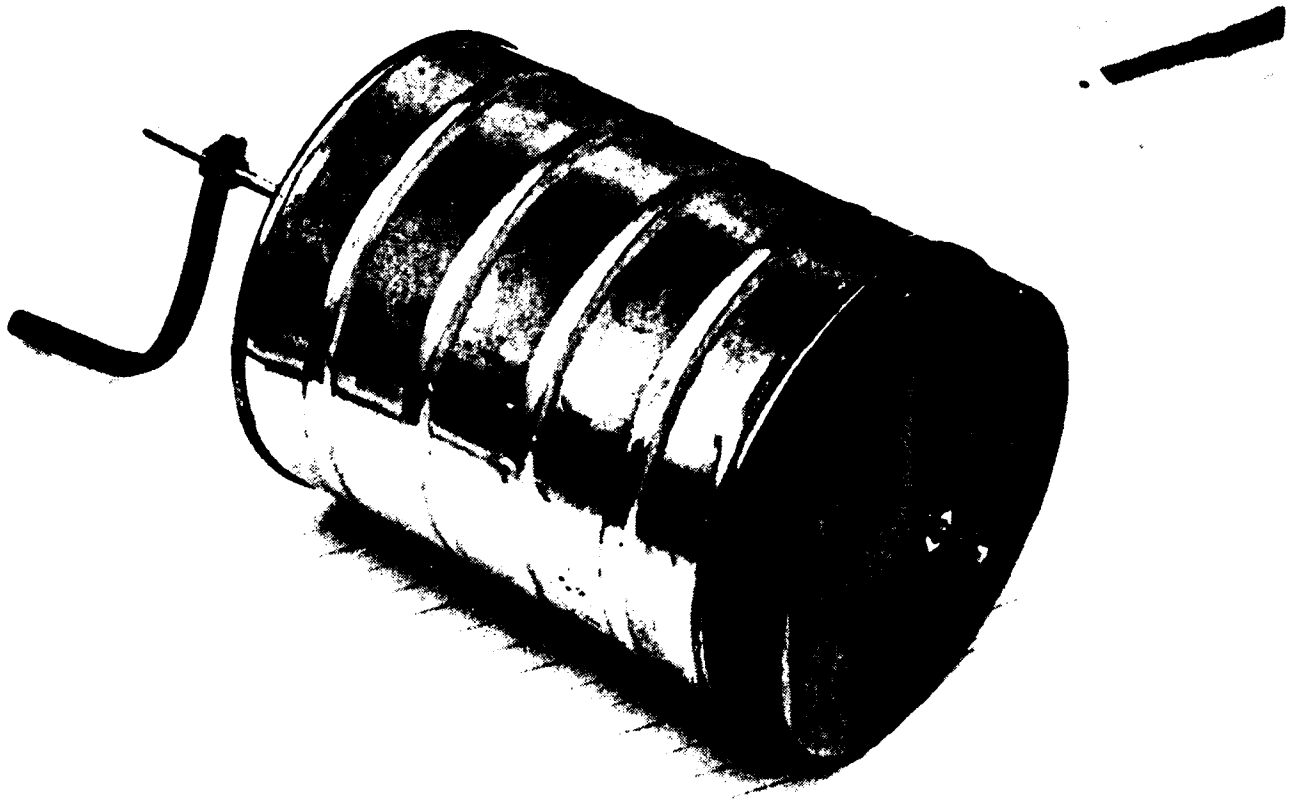

Figure 6 Soot-Slide Sampling Can

inhibiting the formation of measurable impact sites in the soot. It was thought that a slower shutter speed would increase the number of particles hitting the slide and, in so doing, increase the number of measurable impact sites. This slower speed, corresponding to approximately 4 rad/sec rotational velocity for the disk, resulted in an effective exposure time of 0.131 sec.

The slides were observed and measured using a Reichert microscope. Two different objective lenses were used: 11/.25 and 32/.65, with corresponding magnification powers of 9 x and 12.5 x. The projected real image from these lenses was imaged by a television camera mounted on the microscope, and the resulting video signal was displayed on a monitor. When viewed on this monitor, an object having a linear dimension of 100 μm has a dimension of 3.56 cm with the 11/.25 objective lens in place and 9.45 cm if the 32/.65 objective is used. A considerable magnification is thus gained through the use of the video display. The monitor was calibrated by placing a scale with lines 10 μm apart on the stage of the microscope. Initially this image was traced directly onto the video picture tube with short grease-pencil marks along the edge. However, a more precise scale, with horizontal lines crossing the entire screen, was made by placing the micro-scale on the stage of the microscope and carefully measuring the dimensions of the video image. Using these dimensions, lines were ruled onto clear plastic sheets, one sheet calibrated for each objective lens. All slides viewed after 7/12/78 were measured using these overlay sheets on the video screen. Figure 7 is a photograph of the field of view seen in the video image.

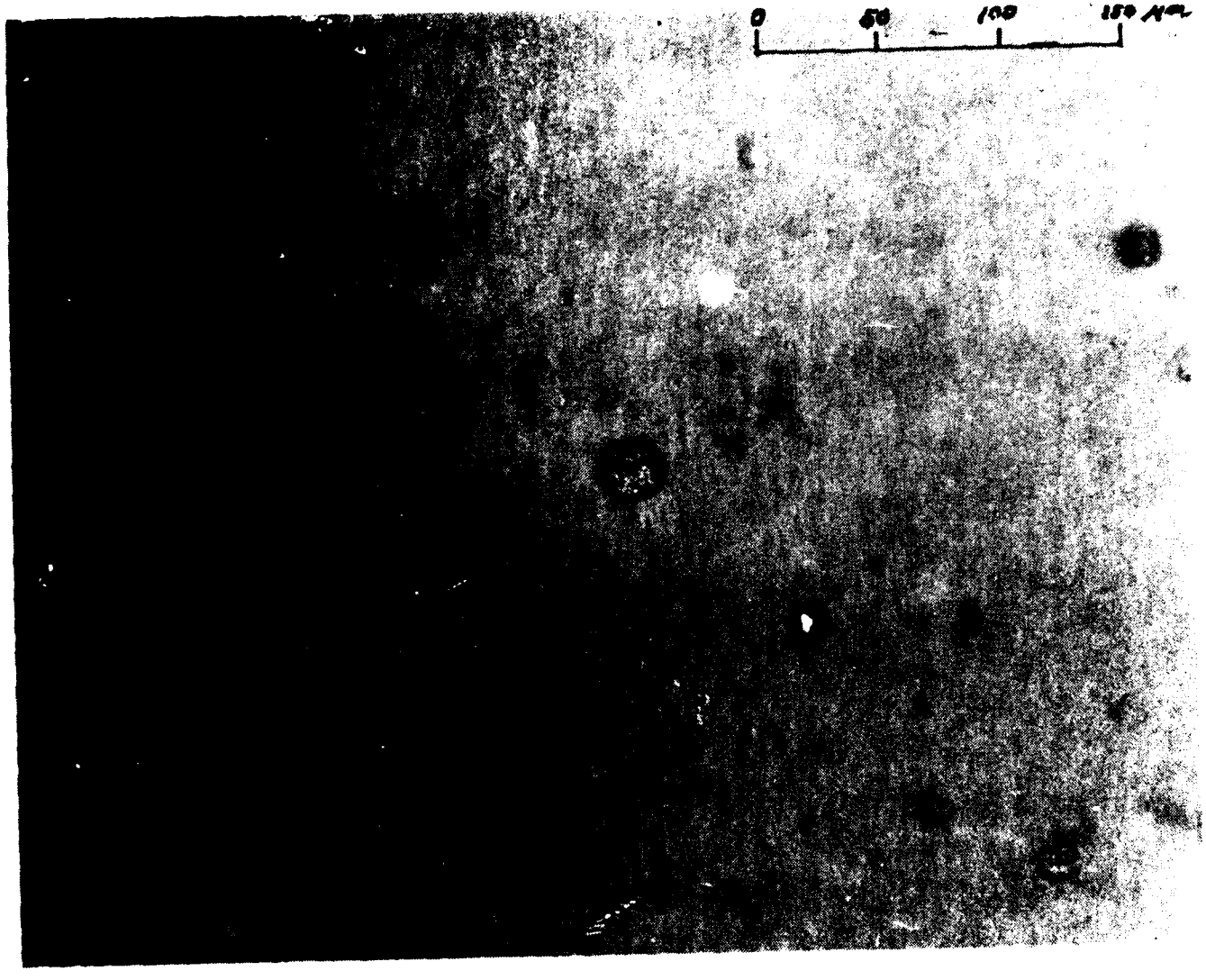

Figure 7 Photomicrograph of Fuel Particle Impaction Sites

Actual samples were taken as follows: (1) An unused slide was placed behind the slot in the wooden disk. (2) The "sampler" was then assembled and placed in the stream. (3) The center of the slide was positioned near the center of the spray, on-axis with the nozzle at a downstream location approximately 30-35 cm, a distance judged to be sufficient for complete development of the spray. (The exhaust fan normally used to dispose of the spray was turned off during sampling so that the only momentum carried by the particles was that which they had upon leaving the nozzle plus that imparted to them by normal air currents or by neighboring particles interacting with them.) (4) After being exposed to the spray, the slides were placed in a cardboard box with a lid, or in a glass sample jar with a lid, and transported to the microscope.

The particle impaction sites, or replicas, were classified according to the size ranges into which they fell. Ranges were 0 through 10 μm, > 10 through 20 μm, > 20 through 30 μm, etc., up to 100 μm, with replicas greater than 100 μm classified simply as > 100 μm. Under reflected light, it was possible to survey the profile of a suspected impaction site by focusing up and down through its depth. A consistent replica was round and had near vertical walls, i.e., a clean "hole" punched in the soot coating. At the very surface of the coating, the edges of the "hole" might be tapered, or beveled; but by focusing deeper into the impression a definite circular outline would appear for a relatively long range of focus, indicating that the outline was the image of a vertical surface, on-axis with the optical system. The diameter of this circular outline was the dimension measured for the replica. An impression size-to-droplet size ratio of 1.05 is given

in the literature (Ref. 4). However, since this correction is small, and its omission gives rise to a larger value for the observed particle size (corresponding to a decrease in injector performance), the value of this ratio was taken to be unity as a conservative estimate.

A mean droplet size for each heating rate was calculated by multiplying the number of observed impaction sites in each size classification by the middle value in that range and dividing the sum of these products by the total number of sites.

Each observed spray at specific settings of heating rate-to-flowrate ratio and downstream pressure drop was assigned a qualitative "rating," based on visual observation, and was recorded photographically. This rating, based on the aforementioned 1-to-10 scale, could not provide quantitative droplet size information; but it was used to furnish a reliable relative index by which changes in the spray appearance could be detected and documented, especially when supplemented by a photographic record.

The non-invasive laser scattering experiments that were conducted following the glass slide observations were the simplest that could be carried out with any expectation of quantitative results. Each test consisted of a straightforward measurement of the attenuation of a single beam along a straight path through the cloud of fuel droplets. By utilizing a well-established solution to Maxwell's electromagnetic wave equations for the case of spherical particles in a monochromatic beam (Mie theory), one can model this experiment analytically; and depending upon the assumptions made, experimental results can be predicted for a range of mean droplet sizes and size distributions. Measured

experimental data are then compared to the analytical predictions; and, if agreement is found, the particular distribution and mean droplet size assumed in the calculations are considered similar to the actual values for the spray in question. The degree to which the simulated conditions may be equated to the actual ones then depends upon how well the following assumptions underlying the Mie theory have been met:

(1) light is scattered by individual droplets only and is unaffected by the spaces between them;

(2) each scatterer is illuminated by the incident beam and not by light scattered from other droplets; and

(3) the scattering elements are spherical.

Assuming these conditions to be satisified, the analytical solution to the attenuation experiment defines the ratio of transmitted beam intensity to incident beam intensity to be:

$$I/I_o = e^{-v\ell}$$

where v = attenuation index $= \int_0^\infty N(a)C(a)da$, and

$N(a)$ = Number of spheres per unit volume of spray having a radius a,

$C(a)$ = Scattering cross-section for a particle radius a,

ℓ = optical path length through the distribution.

Since I/I_o and ℓ are measured quantities which characterize a particular size distribution, a value for the attenuation index can be calculated. Then, based upon an assumed size distribution function, a series of analytical values of attenuation index are computed theoretically for a range of mean sphere radii. Finally, each of these calculated values is compared with the experimentally-determined one; and, if

the assumed size distribution function is correct, the mean droplet radius producing the matching theoretical attenuation index is taken to be the mean radius of the actual droplet distribution.

Measurements of the intensity ratio (I/I_o) and the optical path length (ℓ) were carried out using the apparatus previously described and shown schematically in Figure 5c. With the spray off, the photomultiplier tube power supply was adjusted so that the tube output was 1.00 volts for the unattenuated laser beam. At this same constant supply voltage, the spray was initiated and a measurement made of the tube output for each selected heating rate-to-flowrate ratio. This observed output voltage then corresponds numerically to the intensity ratio.

The externally-mounted scale was utilized to estimate the optical path length by noting that those photons scattered by the cloud of droplets appear to the observer as a thin red line whose approximate beginning and end points could be identified on the scale. An additional check on this estimate was made by photographing each spray in such a way that the laser trace and the scale were both in one frame. These photographs were all taken from a fixed position more than 2 m from the spray in order to minimize parallax errors caused by the fact that the scale was displaced approximately 15 cm radially from the spray axis. It should also be noted that with the measurement of ℓ, the spray cross-sectional area, which is assumed circular, has also been determined.

SECTION IV

RESULTS AND DISCUSSION

A. INJECTOR #1 PERFORMANCE

Injector #1 was initially tested with no nozzle downstream from the injector, and pressure drop characteristics for constant flowrates and various heating rate-to-flowrate ratios are shown in Figure 8. Note that volume flowrate is used but may be changed to mass flowrate simply by multiplying by the density of the fuel at room temperature, .809 gm/cc, since the flowrates used herein are based on the temperature of the fuel entering the flowmeter upstream from the injector. The rating of the fuel spray exiting the injector, a qualitative index representing % mist/10, is shown in Figure 9. No particle size data were taken for this series of constant mass flowrate tests.

Re-examining Figure 8 it should be noted that the points of minimum pressure drop all occur at a heating rate-to-flowrate ratio of approximately 280 J/cc. At atmospheric pressure, with an initial temperature of 21°C, Jet-A fuel begins to vaporize after an enthalpy change of about 310 J/cc. These two numbers are sufficiently close to suggest that the increase in pressure drop following the addition of more than 280 J/cc may be caused by the occurrence of some vaporization within the injector, since this condition corresponds to a rate of heat addition essentially great enough to reach the saturation enthalpy of the liquid fuel.

Figure 9 also has an interesting feature centered about the heat addition point of 310 J/cc. The performance of the spray changes very little up to about 275 J/cc; but above this value, a very small increase

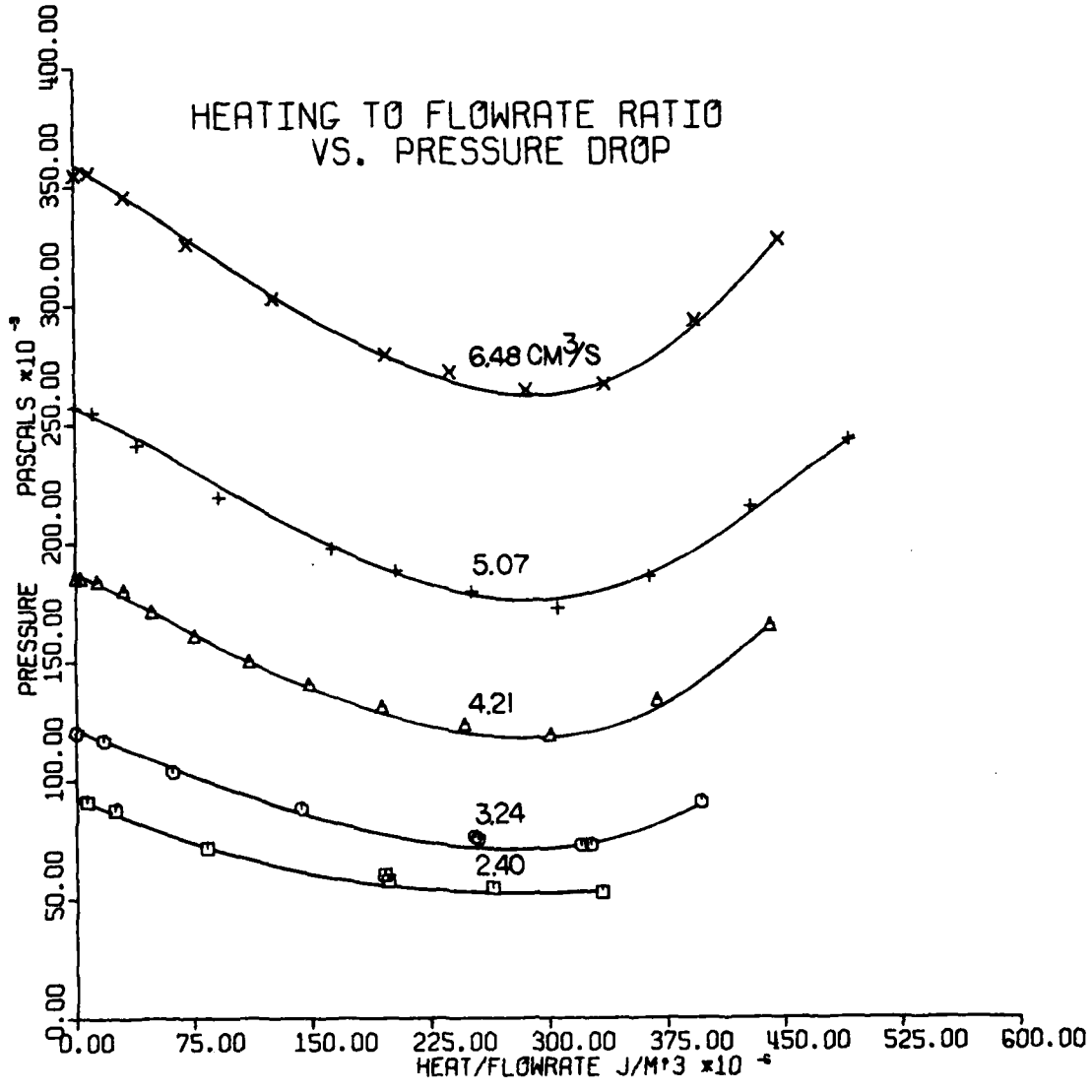

Figure 8 Pressure Drop Characteristics of Injector #1

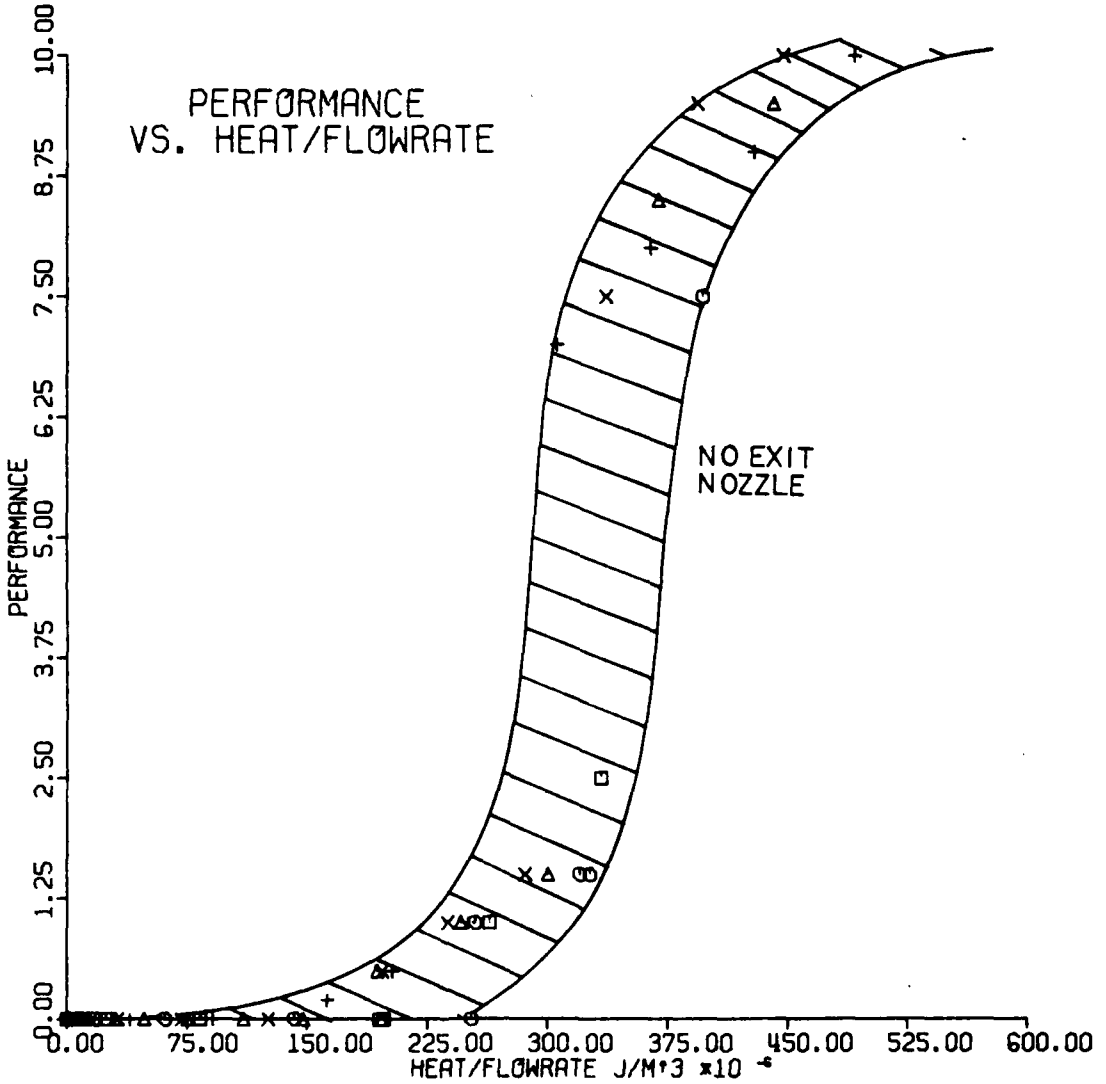

Figure 9 Performance Characteristics of Injector #1

in heating rate causes a relatively large increase in performance rating. In fact, the rating jumps from about 1.3 at 275 J/cc to approximately 9.0 at 400 J/cc, an increase of nearly 600% in rating for a 45% increase in specific heating rate.

B. INJECTOR #1-1

Injector #1-1 was tested with and without a downstream nozzle, with the average nozzle pressure drop equal to 284 kPa. Figure 10 shows the marked decrease in heating rate-to-flowrate ratio required for a given performance rating in tests with a nozzle. Without a nozzle, a rating of 5 required a heating rate of about 350 J/cc, whereas the addition of a nozzle reduced the heating requirement to obtain the same spray quality to about 210 J/cc, a decrease of 40%. This phenomenon occurred in all tests conducted with a downstream nozzle pressure drop and will be discussed in more detail later in this report.

In addition to these qualitative performance observations, attempts were made to measure the mean particle size and droplet size distribution during tests on injector #1-1, and the data from these tests are summarized in Section IV-H, "Particle Size Results."

C. INJECTOR #2-2

Figures 11 and 12 indicate the same pressure drop and spray quality characteristics for injector #2-2 as have already been observed in the performance of injector #1 and #1-1 in tests with no downstream nozzle, namely, a minimum in the pressure drop curve at about 280 J/cc and a rapid increase in performance following a certain critical heating rate-to-flowrate ratio. Here the rating rises from 1.3 at 325 J/cc to

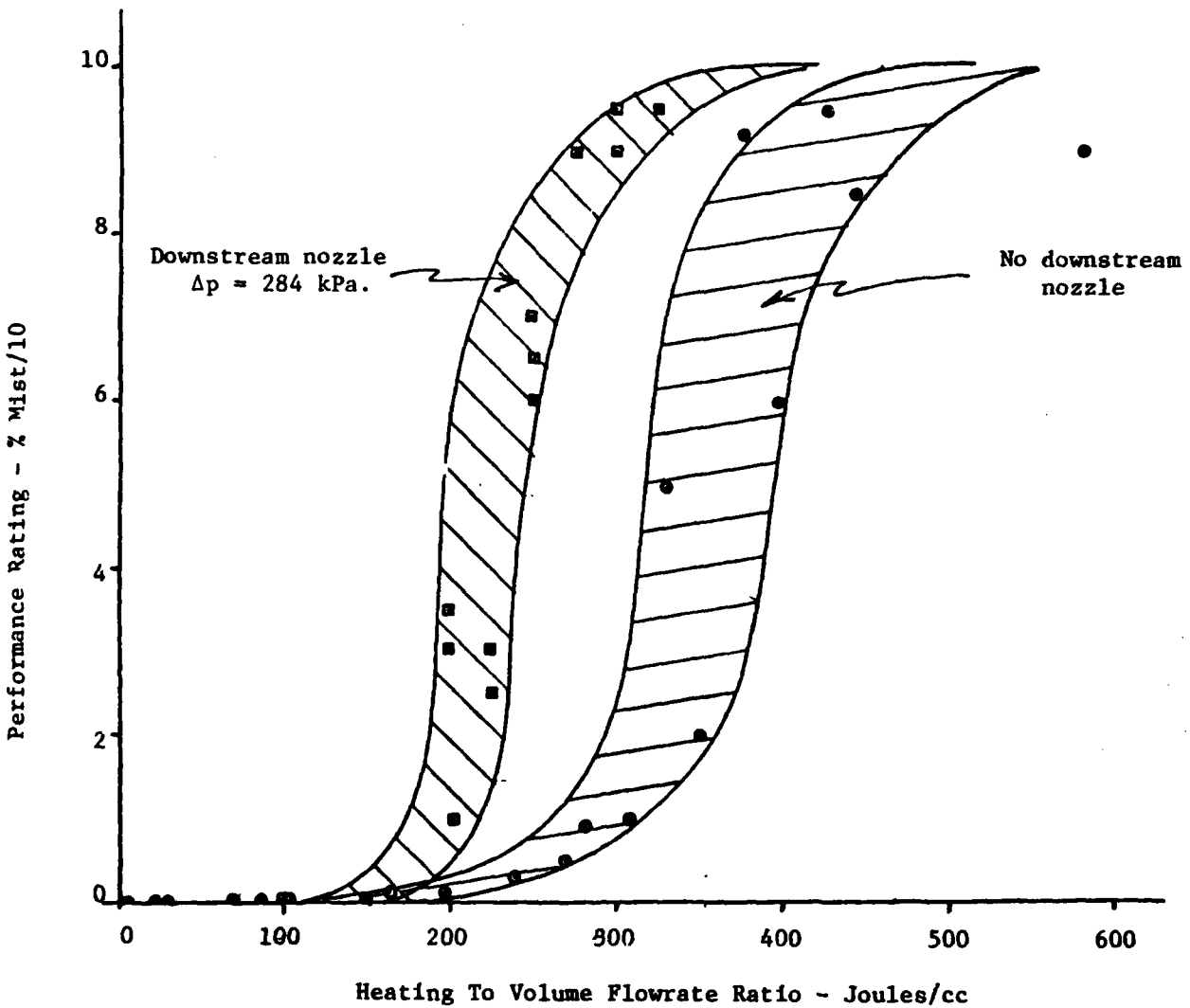

Figure 10 Effect of a Downstream Nozzle on Injector 1 Performance

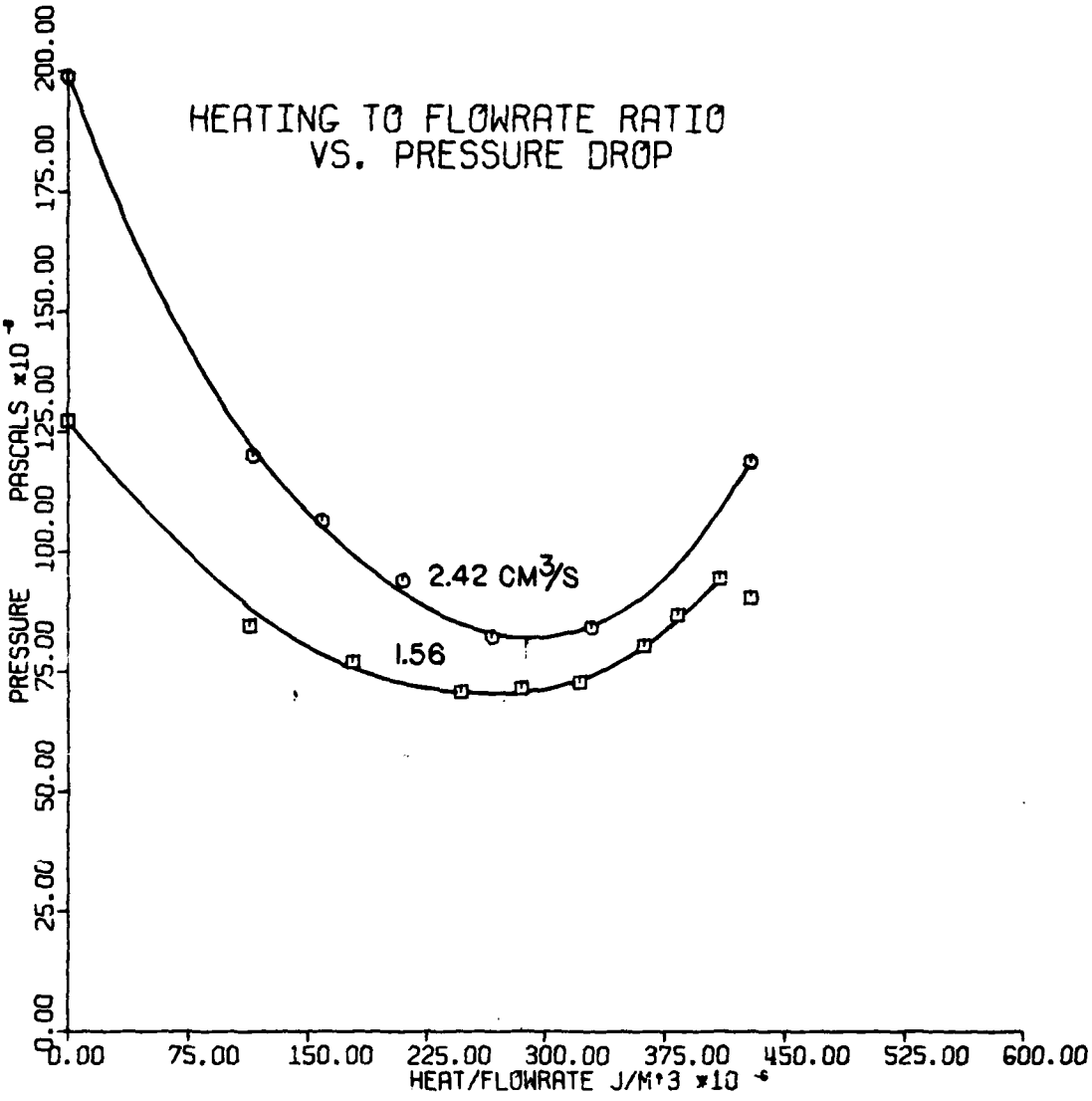

Figure 11 Pressure Drop Characteristics of Injector #2-2

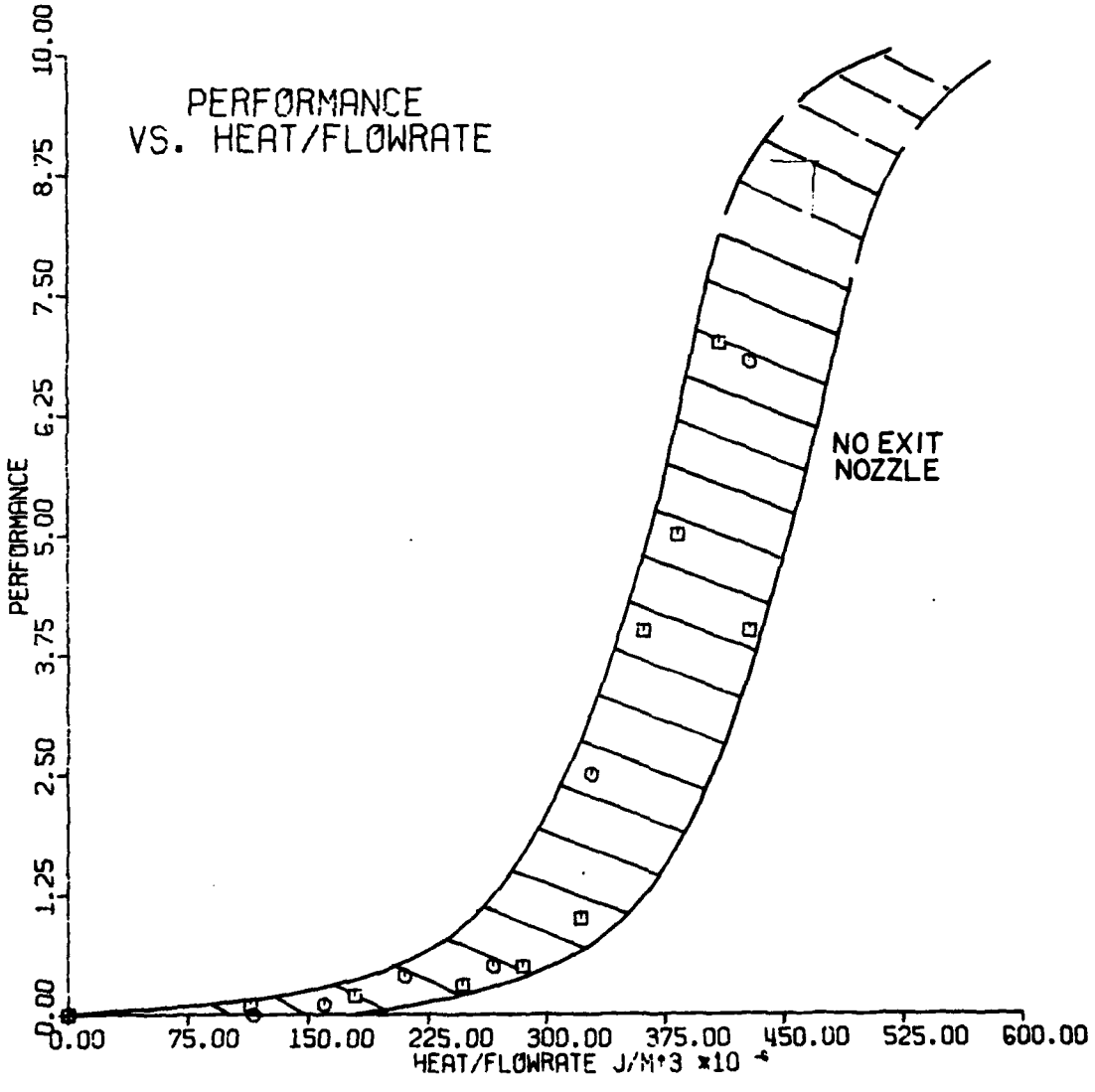

Figure 12 Performance Characteristics of Injector #2-2

9.0 at 450 J/cc, an increase of 600% in performance with only a 38% increase in specific heating rate.

The performance curve for this injector was displaced further to the right on the heating axis than that for injectors #1 and #1-1; i.e., more heat was required to achieve a given rating. Table 1 provides a comparison of the heating requirements of injectors #1 and #2 for a given performance rating. The effect of a nozzle is also clearly shown in this table. On the average, injector #2 required 14.8% more specific heating than injector #1 for any given performance rating.

D. INJECTOR #2-3

The effect of a nozzle downstream of injector #2-3 is shown again in Figure 13. Here a spray performance rating of 5 was achieved with a nozzle at a decreased heating requirement of 275 J/cc, down 35% from the 425 J/cc value without a nozzle. The nozzle pressure drop varied between 20 and 469 kPa for tests on this injector, but the increased performance rating seemed almost independent of the magnitude of the pressure drop. (This was found to be true on all injectors.) The optimum pressure drop was not sought for the nozzles utilized herein, since there had been no attempt to optimize their geometry in relation to the characteristics of the fuel or the flow rates.

The pressure drop characteristics exhibited by this injector are shown in Figure 14. The minimum in the pressure drop curve that was characteristic of tests on injectors #1 and #2-2 is found in only one of the eight flowrate conditions tested, viz., in one of the two flows in which the downstream nozzle was not present (1.50 cc/sec and 2.02 cc/sec).

Table 1

Average Heating Requirements for Given Performance Ratings for Both Injectors, With and Without a Downstream Pressure Drop

		Rating of 1	Rating of 3	Rating of 5	Rating of 7	Rating of 9	Avg. % Difference From Inj. 1 to Inj. 2	Avg. %	Avg. %
Average $\dot{Q}/\dot{v}$ for Tests Without a Nozzle - $J/_{CC}$	Injector 1	288	323	340	359	427	13.4	14.8	---
	Injector 2	305	355	395	442	527			
Average $\dot{Q}/\dot{v}$ for Tests With a Nozzle - $J/_{CC}$	Injector 1	197	213	238	258	293	16.4		
	Injector 2	225	255	293	308	357			
Percent Decrease in $\dot{Q}/\dot{v}$ (from Nozzle)	Injector 1	32	34	30	28	31	---	31.0	29.7
	Injector 2	26	28	26	30	32	---	28.4	

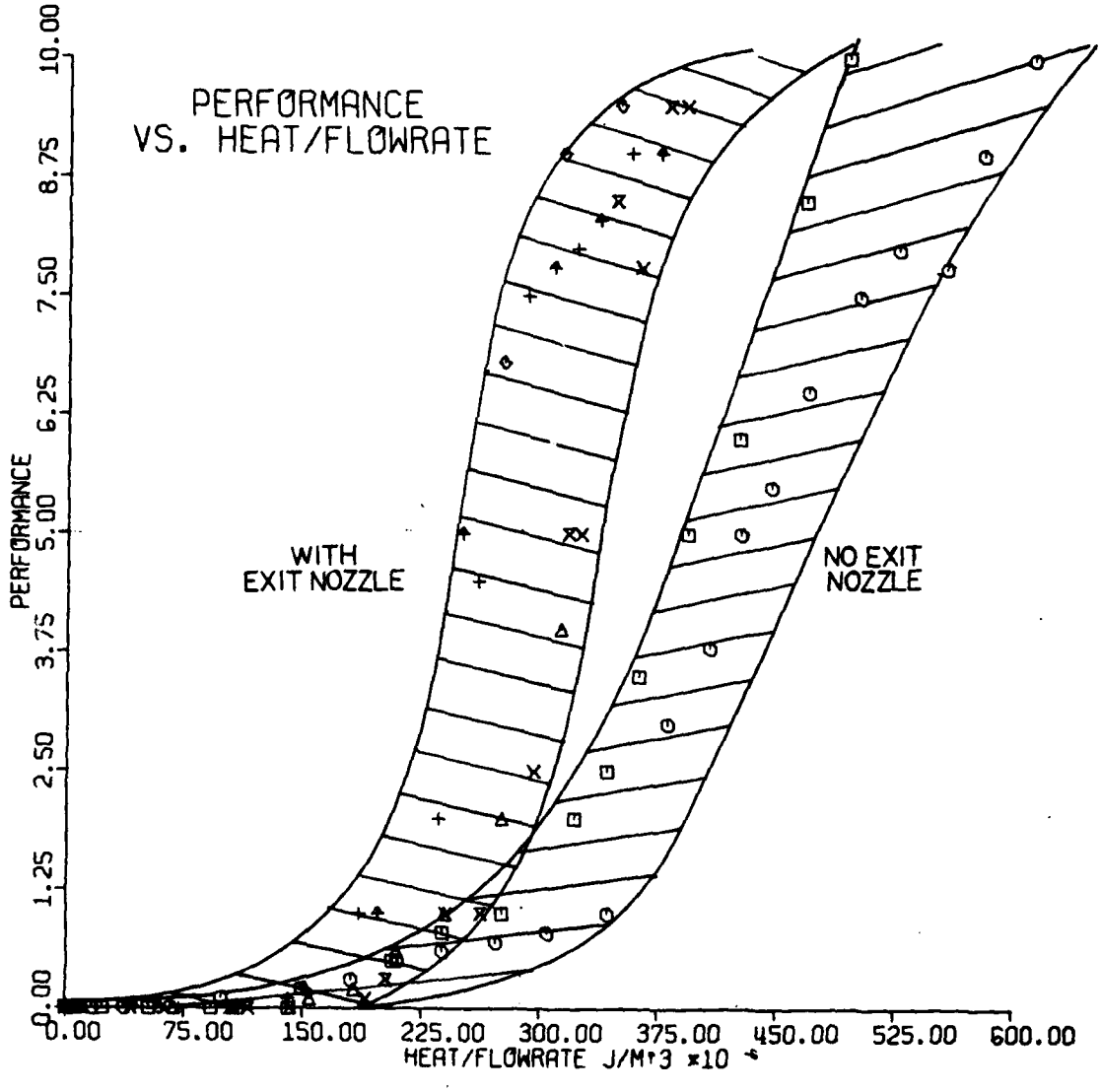

Figure 13 Performance Characteristics of Injector #2-3 With and Without a Downstream Pressure Drop

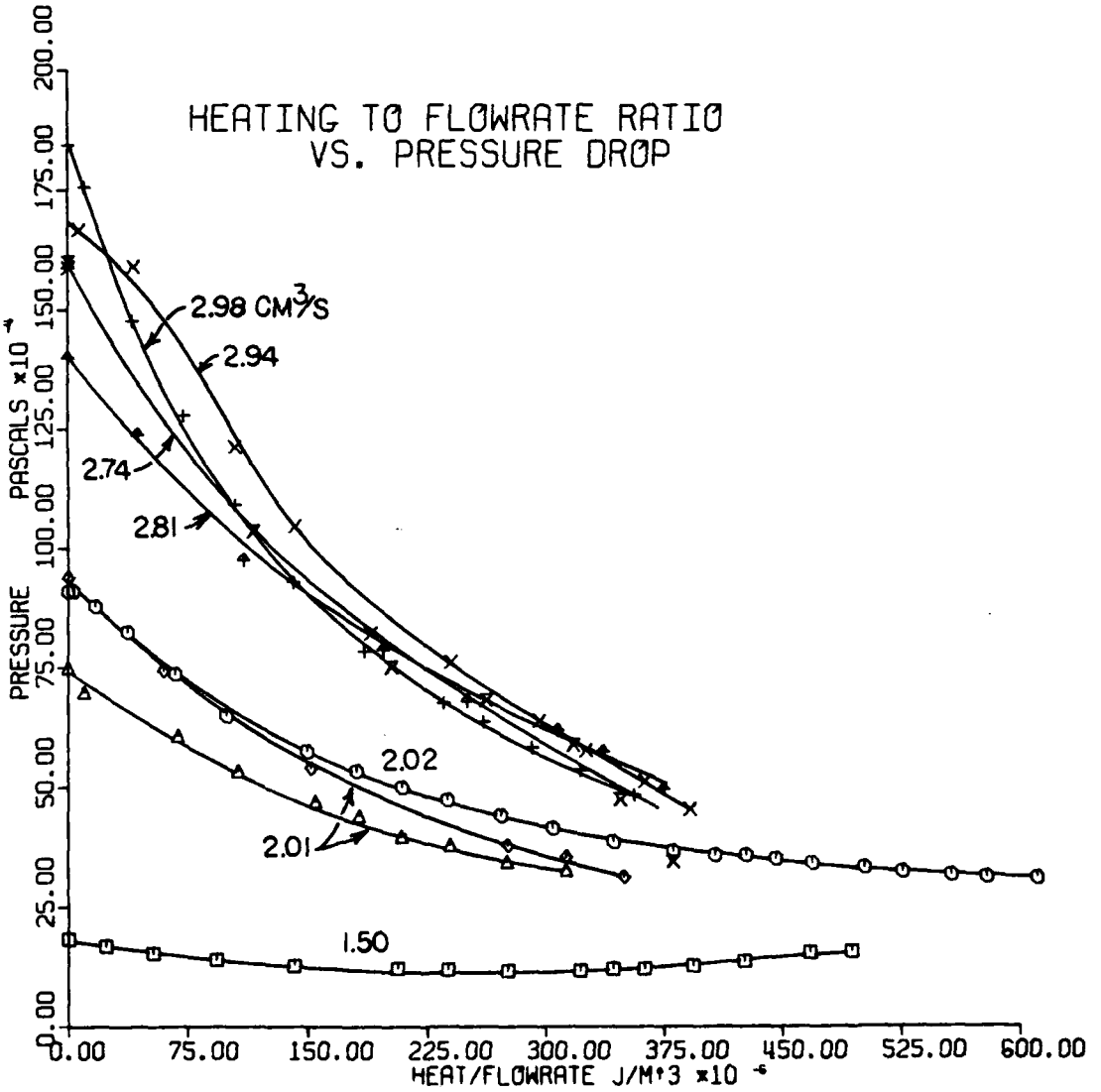

Figure 14 Pressure Drop Characteristics of Injector #2-3

It should be noted that the scale of pressure drops on Figure 14 ranges from 0 to 2,000 kPa, a factor of 10 larger than that of Figure 11, and five times as large as the scale of Figure 8. This abnormally high pressure drop phenomenon was not studied in detail, but apparently the injector became partially clogged. This clogging could be due to a number of circumstances such as thermal cracking of the fuel with subsequent gum formation or "coking," compression of the metal whiskers within the injector volume, or bulk thermal expansion of the whisker volume at the elevated temperatures encountered during testing. Order of magnitude analyses of all these possible phenomena were carried out in order to isolate the most probable causes of the observed increase in pressure drop.

The problem of coking or gum formation is of significant interest with the SFI since its performance depends so heavily upon the addition of heat to the fuel. Although the measured liquid or spray temperature reached at the exit of the injector was generally below 250°C, there were several instances during the early testing phases in which local fuel temperatures could have exceeded 500°C, well above the vaporization and typical cracking values. Furthermore, even in those cases where temperatures were less than 200°C, the time of exposure of the fuel to these elevated levels may have been sufficiently lengthy to permit thermal cracking to occur.

A generalized representation of the cracking process in good quality jet fuels shows that critical exposure times for substantial gum formation decrease logarithmically with temperature rise from values of about

100 seconds at 160°C to 10 seconds at 210°C. In the experiments involving injectors #1-1 and #2-3, overall residence time of the fuel in the flow passages did not exceed 10.4 seconds, based upon the minimum tested flowrate of 1.25 cc/sec; and certainly the average time of exposure to very high temperatures was substantially below this value. Nevertheless, it is possible that a local spot within the whisker network had a lower porosity than the average, causing the fuel to decelerate within that passage and thus to experience longer-than-average residence times.

In some of the earliest tests, temperatures clearly exceeded the minimum for excessive gum formation, even at relatively high flow rates; and it is likely that this phenomenon was a major factor contributing to the high pressure drops encountered in some of these tests as well as to the observed increase of pressure drop from one test to the next. Obviously, then, tests of a continuing nature should only be performed if the temperature does not exceed about 200°C, especially for an experimental setup in which the fuel is collected and re-used.

A related problem observed in a few tests was the time dependency of pressure drop for a constant flow rate even when no heat was added to the injector. This behavior was probably due to a spring-like whisker network which compressed slightly, and inelastically, with the application of pressure, creating an apparent decrease in porosity with time. During testing, it was not always evident that the pressure drop for any given flowrate and heating rate was approaching some final, constant value, particularly in the case of injector #2. According to one of Prof. Schladitz's co-workers, this injector may not have had the whiskers as well packed into the annular ring (Figure 4b) as originally designed;

and even after approximately 100 hours of total test time, the pressure drop across this injector was still increasing, albeit slowly enough to conduct a meaningful experiment.

In addition to gum formation and possible shifting of the whisker network resulting from different inlet pressures and flows, the volume change of the whiskers due to thermal expansion should be examined. The extreme condition in this situation would be that in which the injector volume remained unchanged while the whisker volume expanded, thereby reducing the effective porosity. Assuming an average bulk coefficient of thermal expansion for nickel of 13×10^{-6} per °C, with a maximum temperature rise of 260°C, the change in porosity is approximately 0.25%, which is clearly a negligible decrease when compared to the several-fold increases in observed pressure drop. Thermal expansion can therefore be eliminated as a possible contributing factor.

E. COMPARISONS OF PRESSURE DROP CHARACTERISTICS

Figures 8 and 11 both show a minimum in the pressure drop across the injectors at about 280 J/cc when there is no nozzle downstream of the injector exit. At a flowrate of 1.50 cc/sec, a test also performed without a downstream nozzle and the only curve in Figure 14 demonstrating a pressure minimum, this minimum was again reached at about the same 280 J/cc heating rate. These results can be intepreted with the help of the enthalpy diagram for Jet-A fuel, Figure 15 (developed from Refs. 1, 2, 3), and with the control volume schematic diagram for a Schladitz Fuel Injector, Figure 16. Point A on Figure 15 is the initial vaporization point for Jet-A fuel at atmospheric pressure. At that pressure, any heat applied to the fuel that causes the enthalpy to exceed 365 J/cc

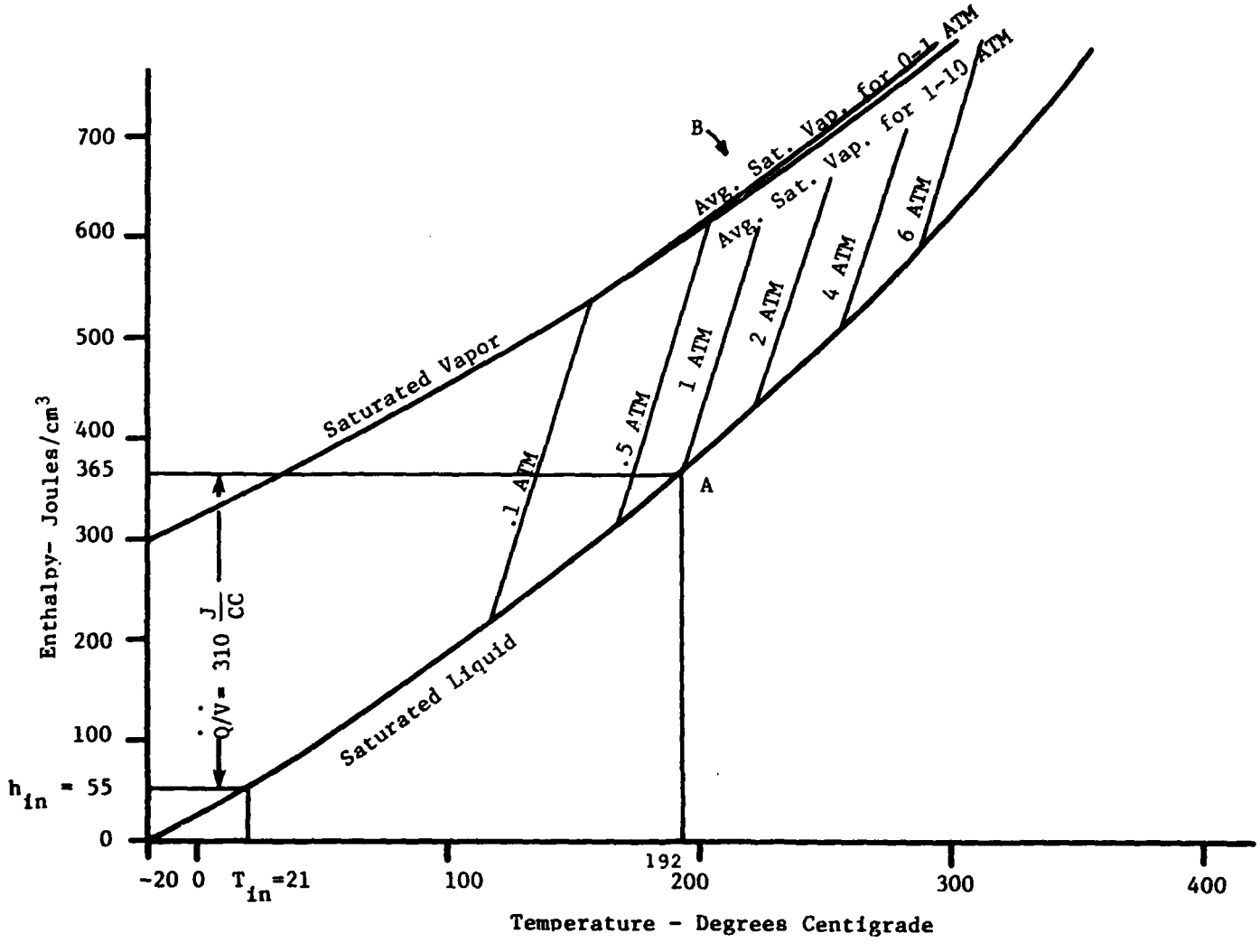

Figure 15 Approximate Enthalpy Diagram for Jet-A Fuel

will result in some vapor formation. Figure 16 shows this change in enthalpy for the fuel. If it is assumed that all of the energy supplied to the injector heating coil reaches the fuel, then the enthalpy change for any test on the SFI can be approximated as the sum of the heating rate-to-flowrate ratio and the enthalpy of the fuel entering the injector at room temperature, 55 J/cc. This value of enthalpy can then be used on Figure 15 to find the thermodynamic state (liquid, vapor, or mixture) of the jet fuel spray if either the downstream pressure or temperature is known.

It was suggested earlier that the increase in pressure drop across the injector for a given flowrate at heating rate-to-flowrate ratios above 280 J/cc was due to internal vapor formation. This can only be speculated, since the pressure drop across the injector occurs continuously through the length of the injector; and, similarly, the heating takes place over the entire length of the injector. Vapor formation may possibly occur only at the very end of the injector flow channel, if at all, in which case the increased pressure drop is not explained adequately by this model. However, the repeatability of the experimental results, and the close agreement between the enthalpy change required for vaporization and the actual amount of heat addition (280 J/cc at the minimum pressure drop), indicates that the existence of fuel vapor may be a valid explanation. As a further test of this hypothesis, the experiments performed with a nozzle downstream from the injector (all flowrates except 2.02 and 1.50 cc/sec in Figure 14), can be examined in more detail. At a pressure drop across the nozzle of one atmosphere

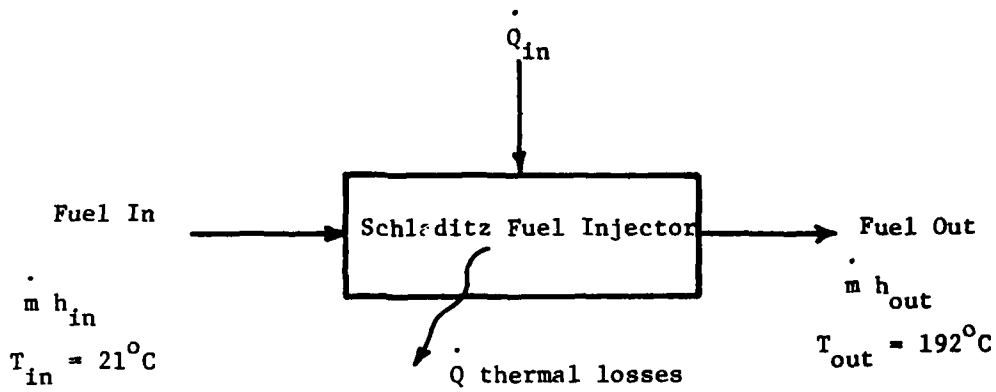

$(h_{out} - h_{in}) = 306$ J/cc (163 Btu/lbm) For $\dot{Q}_{loss} = 0$

Figure 16. Fuel Injector Control Volume Showing Jet-A Enthalpy Change Required to Start Vaporization of the Fuel (at Atmospheric Pressure)

(~100 kPa), the heating rate-to-flowrate ratio required for vapor formation within the injector is 430 J/cc - 55 J/cc = 375 J/cc, (see Figure 15) an increase of 65 J/cc over the heat addition required to reach the saturated liquid point at atmospheric pressure. If enough heat were applied for vapor formation at higher pressures, then the minimum pressure drop points would occur at higher heating rate-to-flowrate ratios, the ratio for each minimum point depending upon the nozzle pressure drop. The curves in Figure 14 (except that for 1.50 cc/sec) are consistent with this prediction in that larger heating rate-to-flowrate ratios would be expected to characterize the minimum pressure drop points if they were to occur in the extrapolated curves. Large pressure drops across the injector itself, even without a downstream nozzle, could also cause the change in the location of the minimum point. (This may be the reason that the test at 2.02 cc/sec showed no such minimum.) Thus, the inhibition of vapor formation due to a combination of nozzle pressure drop and high injector pressures is the most probable cause for the disappearance of the pressure minima in Figure 14.

F. EFFECT OF DOWNSTREAM NOZZLE ON INJECTOR PERFORMANCE

Table 1 provides a method for comparing injectors 1 and 2 in tests with and without a nozzle. In all cases, the effect of the downstream pressure drop was to decrease the heating requirements for a given performance rating, with an average decrease over all ratings of approximately 30% for both injectors.

The performance effect of a downstream pressure drop can be examined in the light of the vaporization hypothesis with the following example, making use of the enthalpy diagram of Figure 17.

A. Without an exit nozzle	B. With an exit nozzle
Rating = 9.5	Rating = 9.5
$\dot{Q}/\dot{v}$ = 412 J/cc	$\dot{Q}/\dot{v}$ = 328 J/cc
$\Delta P_{inj.}$ = 380 kPa	$\Delta P_{inj.}$ = 585 kPa
ΔP_{nozzle} = 0	ΔP_{nozzle} = 288 kPa (2.84atm)

For case A, the fuel discharging from the injector is represented by point 2 in Figure 17. A linear interpolation along the 1-atmosphere isobar indicates a spray quality of 34% vapor. (Note that this calculation assumes that all of the electrical energy supplied reaches the fuel.) For Case B, the fuel entering the nozzle must be represented by point 3' in Figure 17, corresponding to a state of compressed liquid. Assuming an isenthalpic expansion across the exit nozzle, the final state of the fuel is represented by point 3, a mixture containing about 4% vapor.

The results given by this example are typical of those observed in all injector tests. Test results from the experiments indicate that the presence of a downstream nozzle would significantly reduce the amount of, or eliminate all of, the vapor in the stream entering the atmosphere. This suggests that the high degree of atomization observed when a nozzle is placed downstream of the injector is not due simply to vaporization of the fuel within the injector. When there is no downstream nozzle, however, a significant proportion of the fuel must be vaporized to create

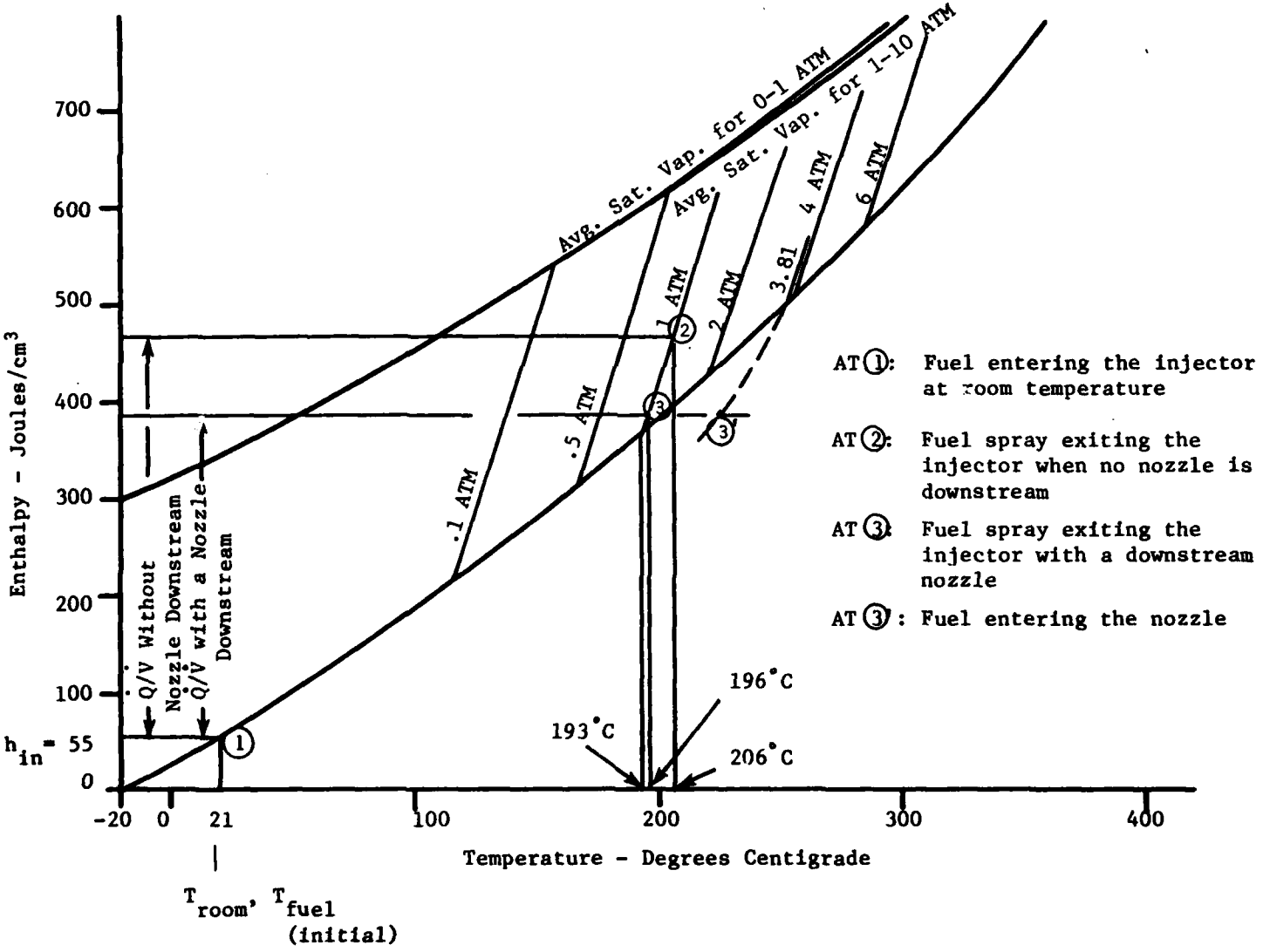

Figure 17 Enthalpy Diagram Showing a Typical Decrease in Specific Heating Requirements Due to a Downstream Pressure Drop

a fine mist. On the average, a rating of 9 for injector 1, with no nozzle downstream, required 427 J/cc of specific heat addition, enough to vaporize 33% of the fuel. However, this same rating was attained with only 293 J/cc for tests with a nozzle, which is not enough heat to vaporize any of the fuel. For injector 2, a rating of 9 required, on the average, 527 J/cc when no nozzle was present, corresponding to about 71% vapor; while with a nozzle, it required 357 J/cc, enough to vaporize only 17% of the fuel. Thus, the Schladitz Heat Exchanger - Fuel Injector is not simply boiling the fuel to create an apparently finely atomized spray, but rather the metal whiskers are apparently playing a significant role in the atomization of the fuel in addition to merely increasing the heat transfer surface.

Even though the decrease in heating requirements caused by a downstream pressure drop was about the same for both injectors (29.7%), injector #2 required an average of 14.8% more heat than injector #1 to achieve a given performance rating (see Table 1). This difference is demonstrated graphically in Figure 18. Because the geometry and the amount and type of insulation were different for the two injector designs, the fraction of the electrical energy supplied to the coils that actually reached the fuel should be expected to be different (as was the case here) resulting in a difference in performance of the two injectors. Typical photographs relating performance rating and specific heating rate for tests with no nozzle downstream of the injector are shown in Figure 19, while Figure 20 presents similar evidence from tests with a nozzle. These photographs help to clarify the differences in qualitative performance ratings as assigned by the experimenters.

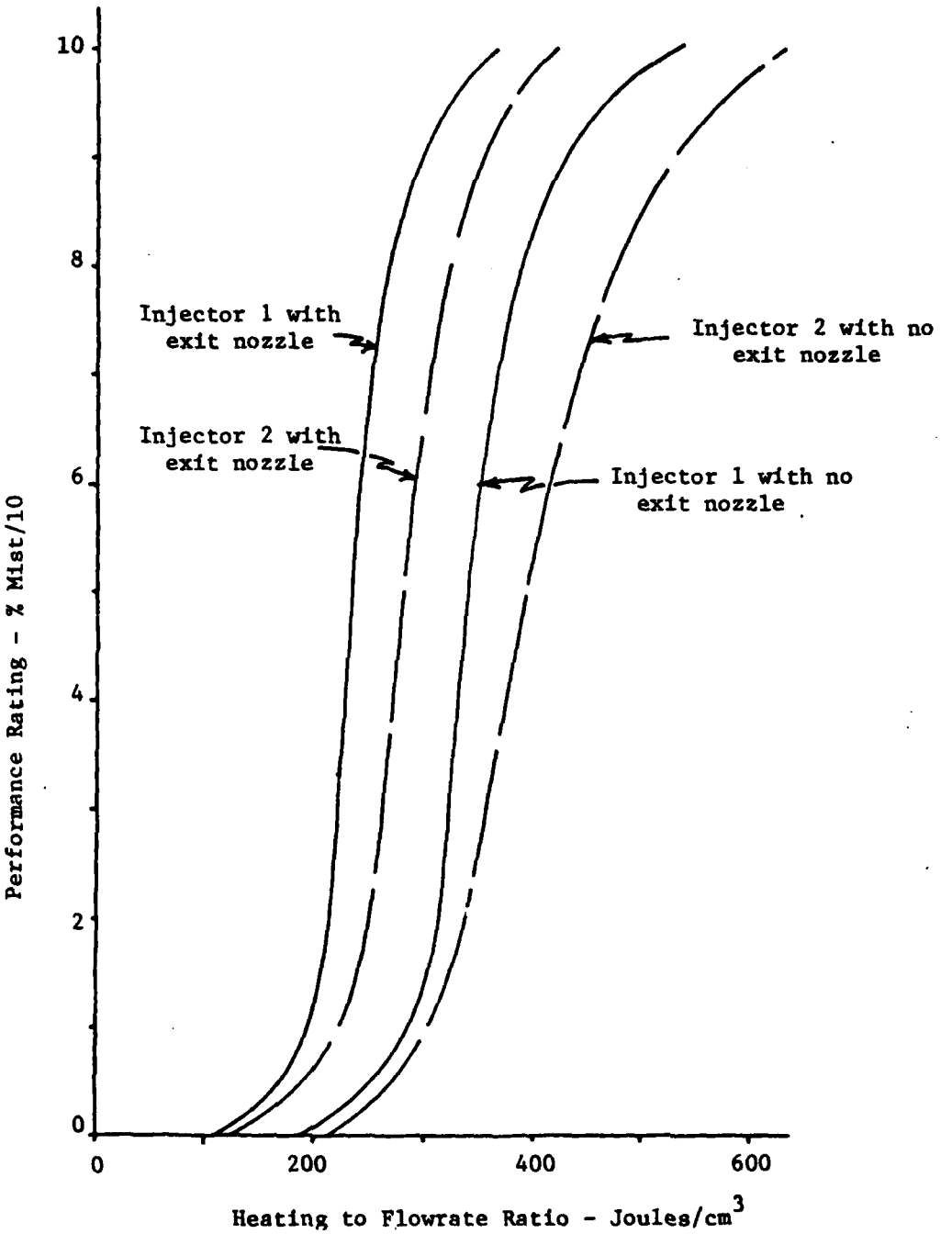

Figure 18 Comparison of Performance Data from Injectors #1 and #2, with and without a Downstream Pressure Drop

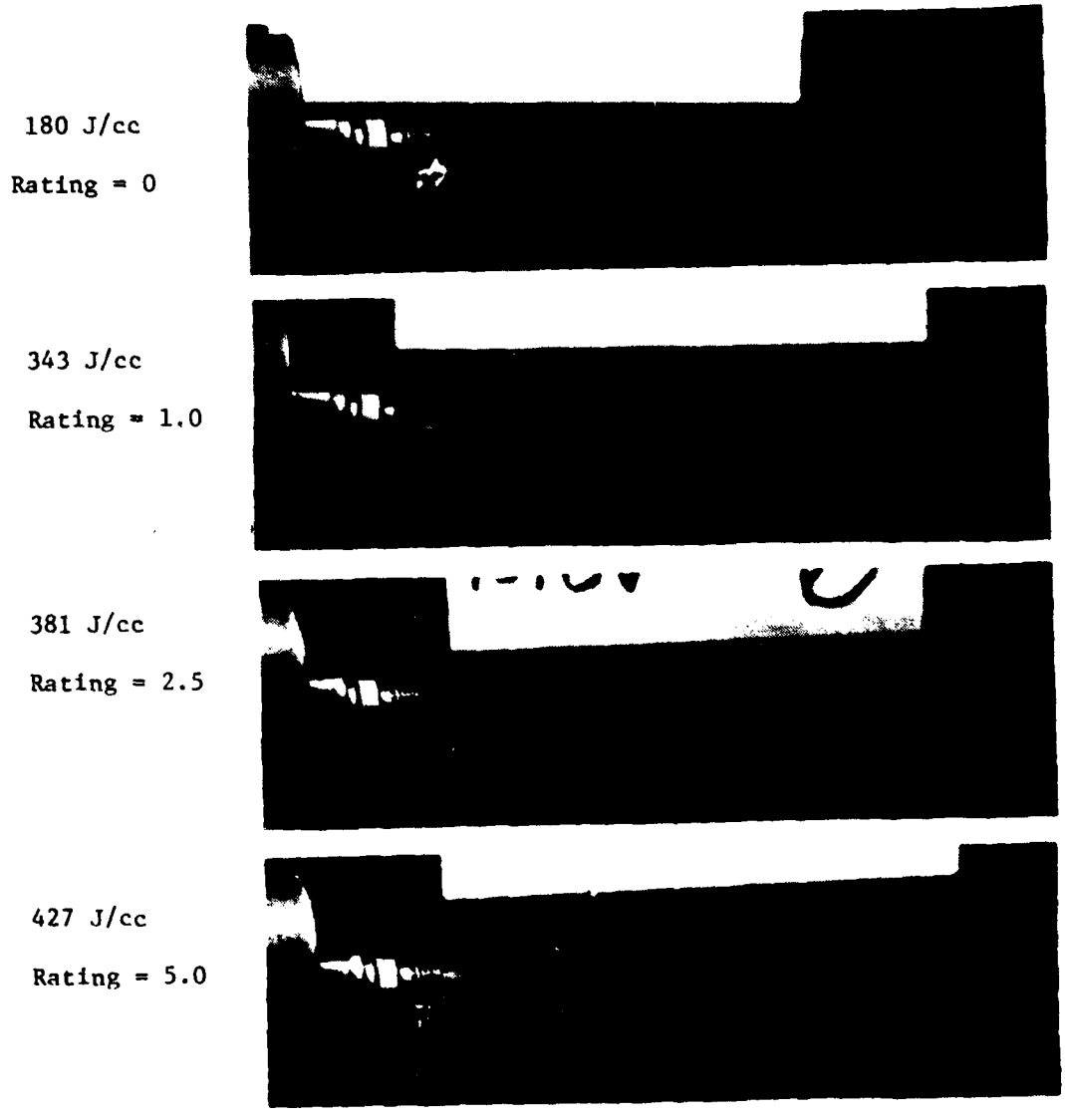

Figure 19 Typical Photographs of a Test with No Nozzle, Comparing Performance Rating and Heating to Flowrate Ratio

469 J/cc

Rating = 6.5

579 J/cc

Rating = 9.0

611 J/cc

Rating = 10.0

Figure 19 cont'd

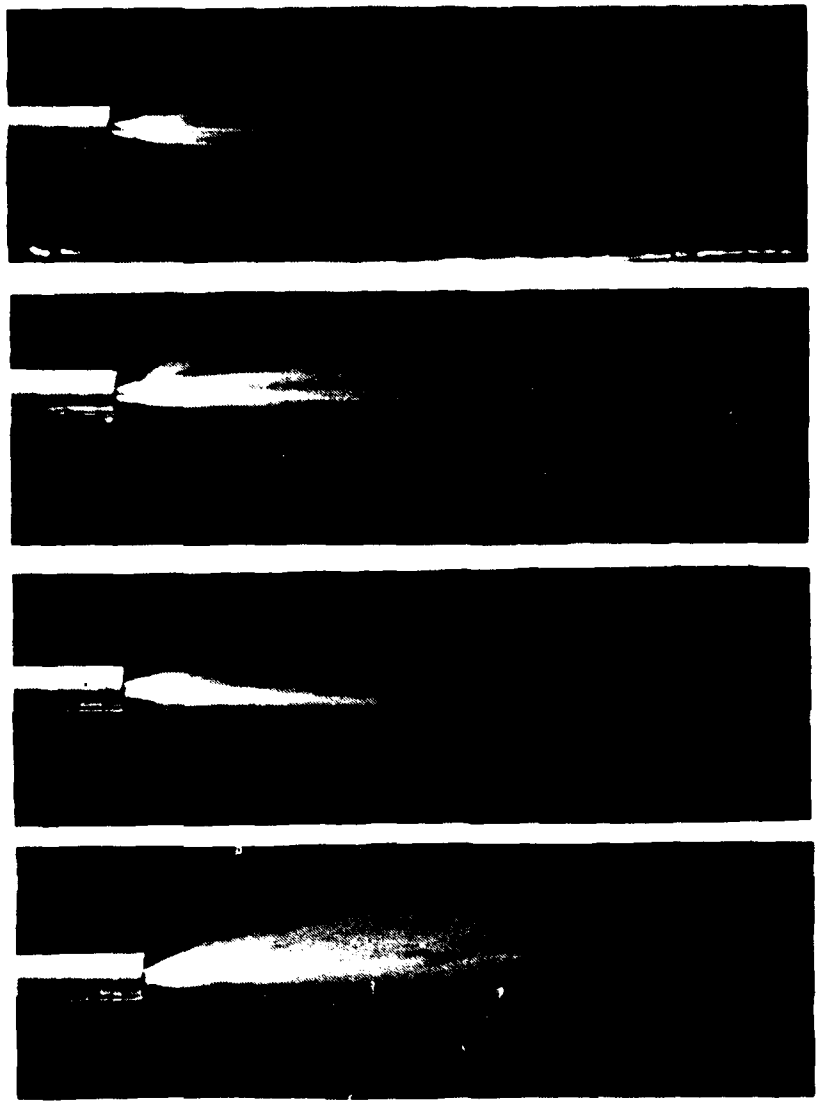

Figure 20 Typical Photograph of a Test with a Nozzle, Comparing Performance Rating and Heating to Flowrate Ratio

250 J/cc

Rating = 7.0

275 J/cc

Rating = 9.0

300 J/cc

Rating = 9.5

325 J/cc

Rating = 9.5

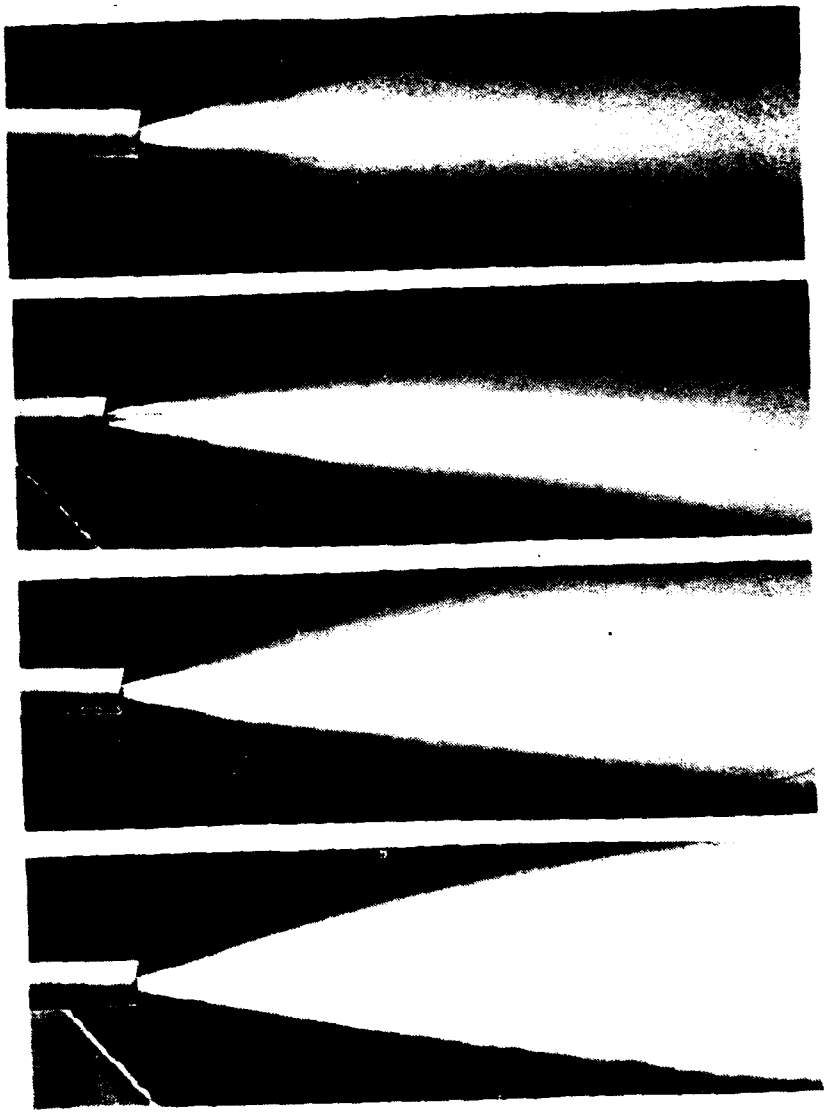

Figure 20 cont'd

G. "COST" OF HEATING THE FUEL

A performance rating of 9 for these injectors corresponds to a very fine mist or fog. If it is assumed that a rating of this magnitude is an indication of an improved combustion process, then the "cost" of such an improvement can be estimated by evaluating the fraction of the heat of combustion that must be put back into the fuel in the form of energy used for heating. (Assume H_v = 10,560 J/cc, or 19,800 $\frac{Btu}{lb}$). The results are shown in Table 2.

The corresponding reduced particle size could be beneficial in three ways:

1) Increased power output from the combustion process utilizing this fuel,
2) Reduced fuel consumption, and
3) Reduced environmentally harmful exhaust emissions.

All of these are interrelated, of course, and some combination of the three would most likely be realized.

The overall improvements in combustion efficiency, specific fuel consumption, and/or exhaust emissions must be sufficient to offset the use of up to 1.6% of the heating value of the fuel (see Table 2). The decrease in engine specific fuel consumption itself may be significant enough to justify the use of such a fuel injection scheme. The cost factor may also be justified as the combustion efficiency is improved and as the need for mechanically-complicated and expensive anti-pollution devices is reduced or eliminated.

Table 2

Percentage of the Heating Value, Hv, of Jet-A Fuel That Must Be Used to Give a Rating of 9, or 90% Mist

Injector Number	1	1	2	2
Downstream Nozzle?	No	Yes	No	Yes
Flow Rating	9	9	9	9
Specific Heat Addition, $\dot{Q}/\dot{v}$, Joules/cm^3	427	293	527	357
Fuel Enthalpy = h = $h_{in} + \dot{Q}/\dot{v} \times .523$, BTU/LBM	257	186	310	220
(% of H_v) = 100 x $\frac{h}{Hv}$	1.30%	.94%	1.57%	1.11%

H. PARTICLE SIZE DETERMINATIONS

The results of the soot slide study on injector #1-1 with a nozzle pressure drop of 283 kPa are presented in Figures 21-26, where it should be noted that the number of particles near the lower limit of resolution (~ 10μm) was found to be greater in sprays that were given high qualitative ratings than those considered to be lower on the performance scale. Figures 21 through 23 show the fraction of particles counted that fell below 10 μm, 20 μm and 30 μm in size, respectively. The number of particles with sizes larger than the effective upper limit of the ability of the method to record size accurately, (~100 μm) was found to be smaller in sprays given a higher qualitative rating (Figure 24).

It is evident from the results presented in Figure 25 that increasing spray quality is accompanied by a reduction in the observed mean particle size. Similarly, the results presented in Figure 26 indicate that increasing the heating rate-to-flowrate ratio results in a reduction in the mean particle size.

Although the value of the mean droplet size measured from the slides seemed to be only a weak function of heating rate-to-flowrate ratio (Figure 26), photographic, laser-scattering, and visual evidence gave rise to the possibility that much more dramatic changes occurred in the spray as the heating rate was increased. The inability of the soot-coated slide to characterize impacting droplets accurately, the spray sampling method, the large droplet measurement limitations, and the method used to view the collected sample each influenced the data, so that the measured value may not have been an accurate representation

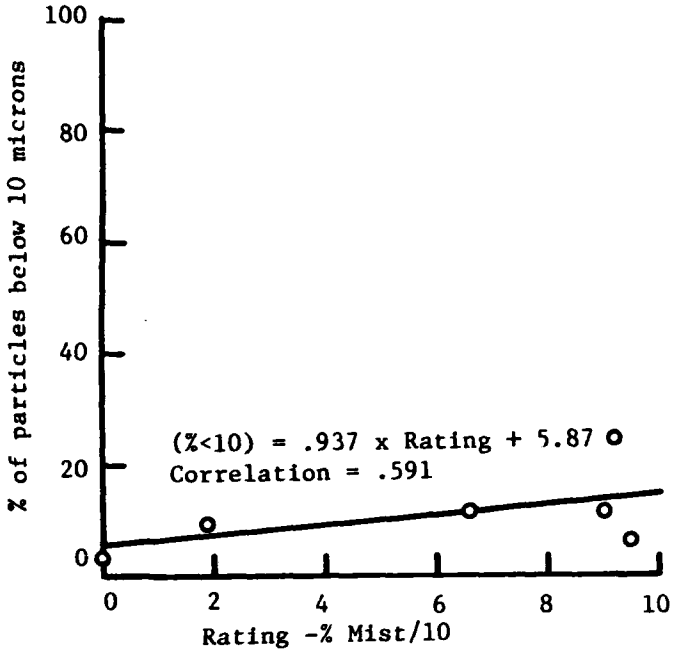

Figure 21 Correlation of Particle Size Distribution with the Qualitative Performance Rating

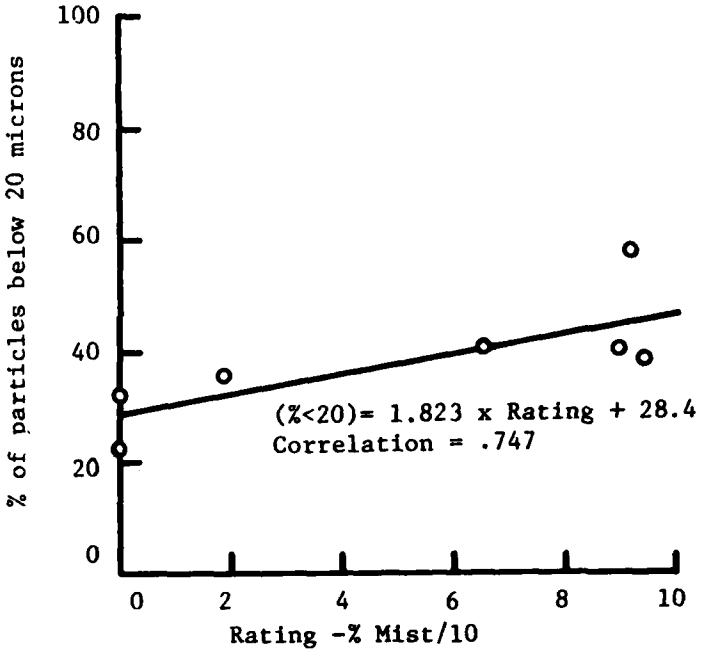

Figure 22 Correlation of Particle Size Distribution with the Qualitative Performance Rating

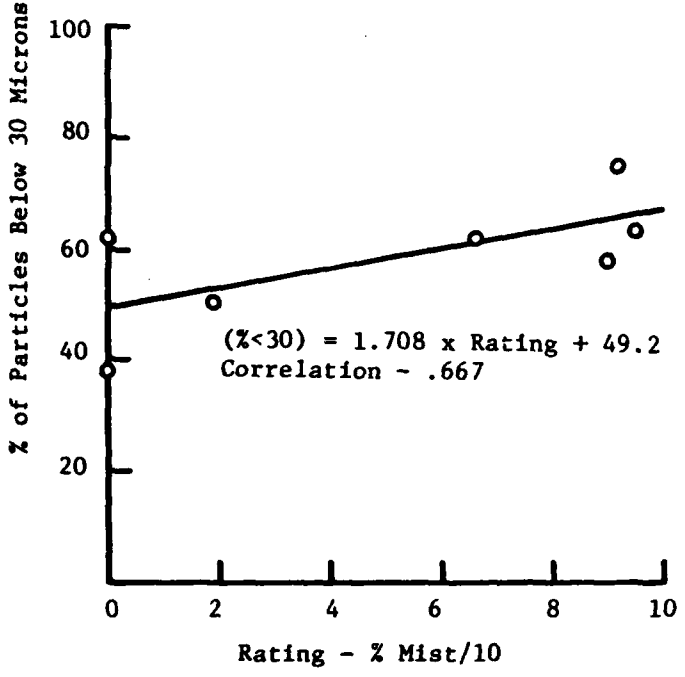

Figure 23 Correlation of Particle Size Distribution With the Qualitative Performance Rating

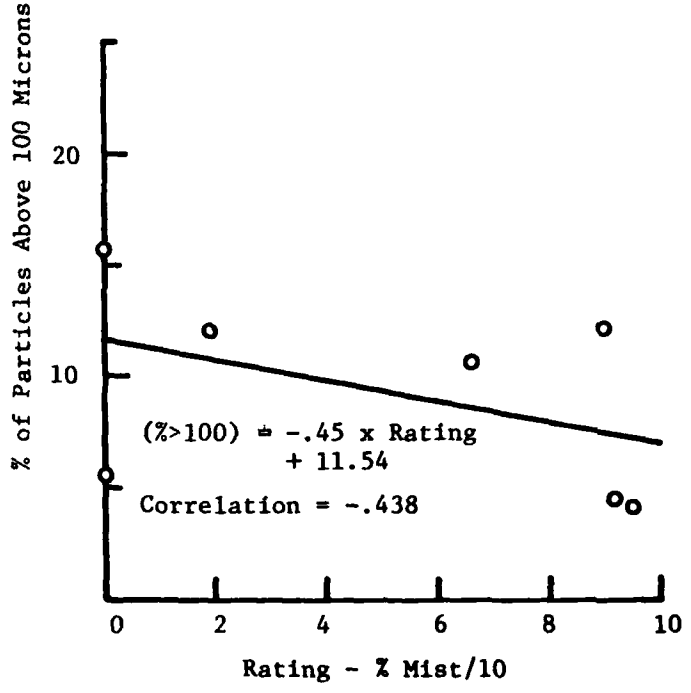

Fig. 24 Correlation of Particle Size Distribution With the Qualitative Performance Rating

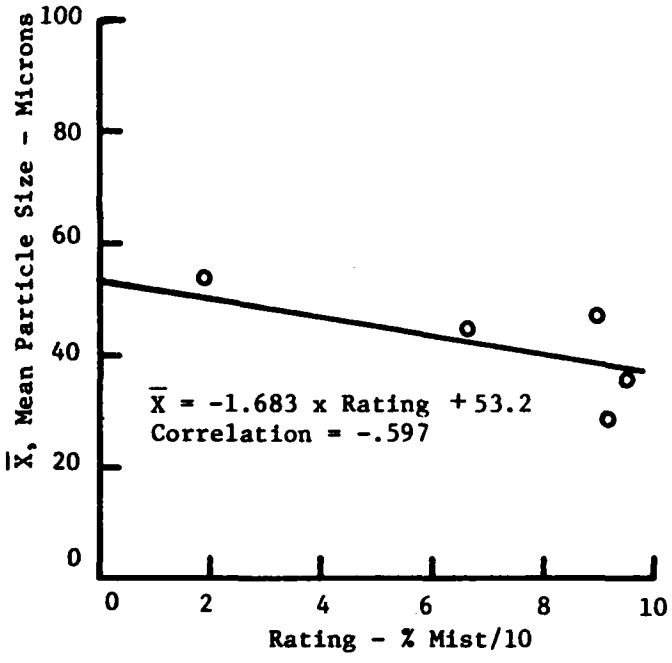

Figure 25 Correlation of Mean Particle Replica Size with the Qualitative Performance Rating

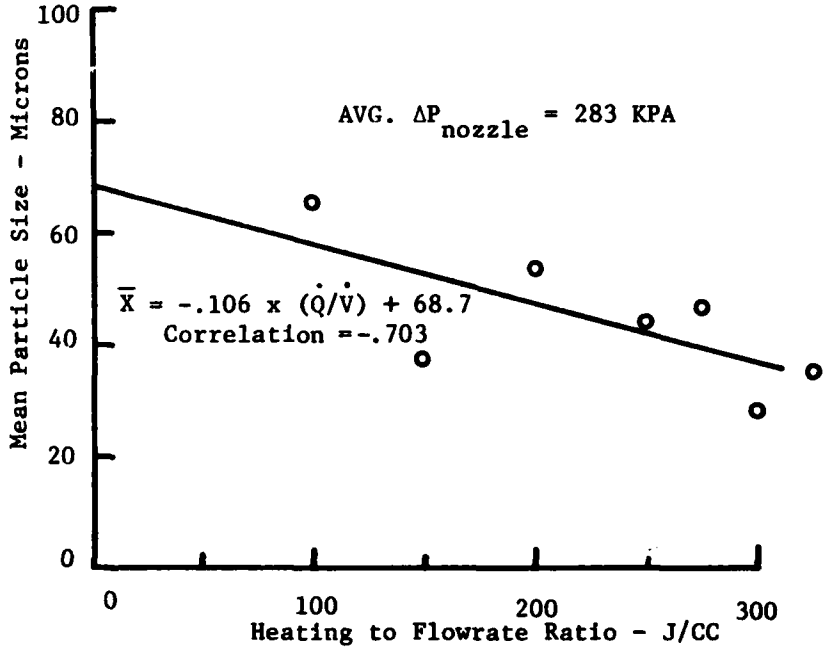

Figure 26 Correlation of Mean Particle Replica Size with Heating to Flowrate Ratio

of the true particle replica size. The possibility of an inaccurate particle size measurement appeared to be strong in the regions of droplet sizes below 10 μm and above 100 μm. At or below a size of 10 μm and at or above a size comparable with the thickness of the soot coating, the replica profiles became irregular and inconsistently shaped. In this size class, anything that resembled a depression in the soot was assumed to be a replica. In the large (> 100 μm) size range, the approximate diameters of whatever impressions existed were measured. Both of these ranges of measurement exhibited a large amount of scatter in the data when compared to other particle size ranges, and it is possible that the values reported for these ranges were in error because of the presence of artifacts (see Figures 21 and 26).

The probability that there were many more particles of sizes less than 10 μm than had been observed was raised by the existence of obviously wetted areas on slides taken in high performance sprays, but with an absence of measurable impact sites. Wetted areas on such slides appeared very rough, similar to what one might expect to see if a very large number of 10 μm sites overlapped each other. Also, researchers in earlier studies have found that an effective lower limit of particle size determination for this and similar techniques is about 10 μm (Refs. 4,5,6,7). Still another indication that there may be large numbers of unrecorded particles smaller than 10 μm is the existence of sample slides with as many as 47% of all counted impaction sites in this size class. The occurrence of these slides was inconsistent with other samples taken under similar flow and heating conditions, and they were therefore treated as anomalies, not to be included in the presentation of results. It was thought that the sample-taking device might be

acting somehow as a particle-size discriminator and in this way, influenced on random occasions by the uncertainty introduced by hand-cranking the shutter, only "small" size particles might reach the soot slide. In an attempt to isolate this possible effect, a number of samples were taken at different "shutter speeds," holding the flow conditions constant. Two different shutter speeds, "normal" and "slower," used at three fixed spray quality ratings (10%, 50% and 90% mist) showed, for 2 ratings, a noticeable increase in measured mean particle size for the slower shutter speed. In the third case (90% "mist") the entire slide was wetted and, under observation with the microscope, seen to be very "rough" on its surface for the slower speed, while for the normal speed a replica size distribution more consistent with previous samples was found. These results reinforce the suspicion that the collection shutter is indeed acting as a size discriminator.

In the range of sizes larger than the soot thickness, the ratio of replica size to particle size increases, i.e., the impression in the soot layer grows relative to the particle size. This raises the possibility that the mean, calculated from impressions made by particles that are above the effective lower limit for soot, is actually lower than reported. On the other hand, as discussed subsequently, laser scattering experiments suggest that a significant fraction of large-sized droplets may have been present at the lower heating rates.

The correction factor from the literature of $\frac{1}{1.05}$ for the ratio of soot replica size to droplet size was not introduced into the data reduction. The resultant implied assumption that replica size equals droplet size is therefore a conservative estimate of the spray characteristics.

The implied existence of many uncounted small (< 10 μm) droplets and the large uncertainties inherent in the soot-slide technique, suggested that an optical scattering system might be the logical next step in the investigation of the characteristics of sprays produced by the Schladitz fuel injector. It was felt that the elimination of uncertainties due to invading the flow of particles might be expected to lead to the development of a more accurate quantitative index of fuel spray performance. Therefore, a straightforward scattering experment consistent with time and resource limitations was chosen, as mentioned in the PROCEDURES section. The results of this investigation were not conclusive in an absolute sense; but they did reinforce previous qualitative observations of the variation of mean droplet size with heat addition to the fuel. Furthermore, the mean size dependency upon heating rate deduced from theory was found to be surprisingly insensitive to the assumed particle distribution function, thus reinforcing the choice of a highly simplified experiment.

Since the Mie scattering theory inextricably binds the mean particle radius, $\tilde{a}$, with its distribution function, N(a), one must either determine these two parameters from a series of independent measurements or assume a knowledge of one of them and derive the corresponding value of the other from experiments. In the first case, it would have been necessary to obtain a large number of laser beam attenuation ratios, I/I_o, each at a known and fixed scattering angle, θ, measured with respect to the direction of the incident beam, and each with its particular optical path length, ℓ, to be determined by separate measurement at

the selected scattering angle. The optimum range of angles is itself dependent upon the probable mean particle size and the refractive index of the fuel spray, so the overall experimental/analytical process becomes one of successive trials or of gaining *a priori* knowledge from other sources before applying the rather complicated theory to a large number of painstakingly-measured intensity ratios. When this experimental complexity is combined with a rather cumbersome computational program that in essence searches for a particular particle distribution function which will optimally match the angular variation of scattering data while still maintaining a mean size consistent with each individual intensity ratio, then the full-blown droplet size determination process becomes almost unwieldy and hardly justified in an exploratory investigation such as this one.

Consequently, a candidate particle size distribution function was sought from previously-obtained soot-slide data in order that the angular variation of intensity ratio might be obviated, allowing mean size to be determined directly from a single observation angle, viz forward scattering ($\theta = 0°$). The fractional numbers of particles classified in each size range, e.g. > 10 to 20 μm, etc., were plotted as functions of size at their mid-size points for each of the three average test flowrates. The results are shown in Figure 27, along with a theoretical density distribution function which exhibits most of the salient features of the soot-slide study and which has been found to be descriptive of many standard fuel nozzle sprays (Ref. 4). This function, called the log-normal distribution, is expressed analytically as (Ref. 8):

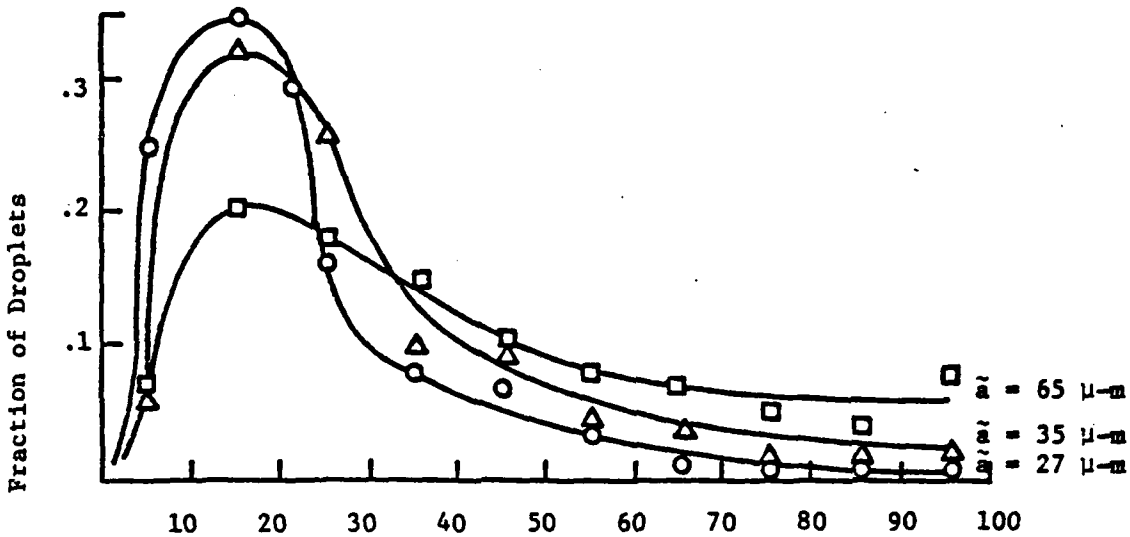

(a) Soot Slide Study Results

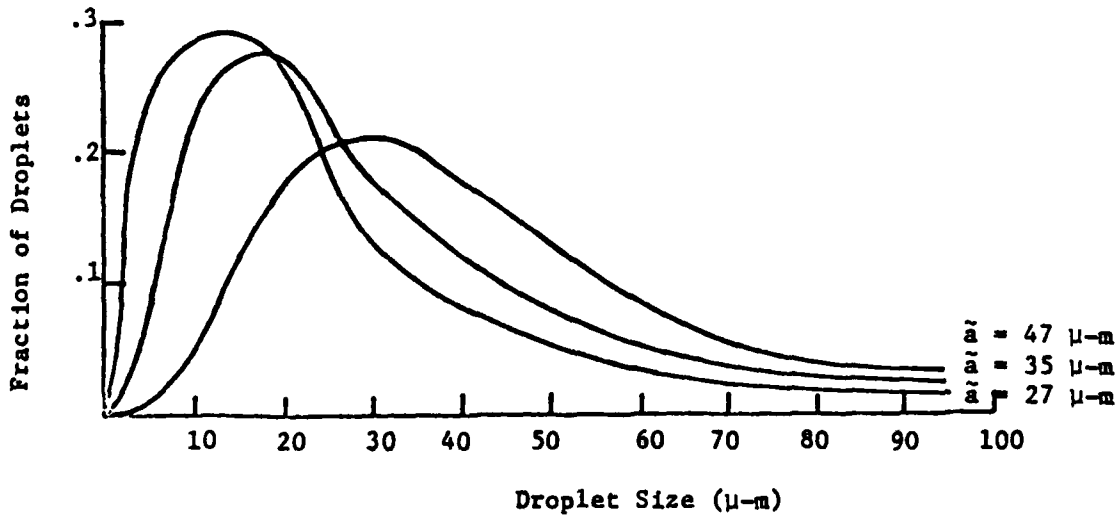

(b) Log Normal Distribution

σ = 30 μ-m

Figure 27. Experimental and Theoretical Particle Size Distributions

$$f(a) = \frac{\exp\left[-\frac{1}{2}\,\frac{\ln\left(\frac{a}{\bar{a}}\right) + \sqrt{\ln\left(\frac{\sigma}{\bar{a}}+1\right)}}{\sqrt{\ln\left(\frac{\sigma}{\bar{a}}+1\right)}}\right]}{a\sqrt{2\pi\,\ln\left(\frac{\sigma}{\bar{a}}+1\right)}},$$

where σ is the standard deviation.

Utilizing this (or any other) prescribed distribution function as an input, the mean droplet radius corresponding to each measured intensity ratio was calculated from Mie theory, utilizing a Fortran program on the Cyber 72 computer. The variation in this mean size determination with changes in the heating rate-to-flowrate ratio is shown in Figure 28 for the log-normal distribution. The most striking feature of these results is the strong dependence of mean droplet size on the heating rate at any flowrate. In the range of interest, from about 150 to 300 Joules/cc, the predicted mean size decreases nearly four fold. If these results are reasonably accurate, the dramatic improvement in spray quality described earlier on a rather coarse rating scale is certainly a reasonable expectation.

The large discrepancy between the calculated mean droplet size (Figure 28) and the soot-slide measured values at very low heating rate-to-flowrate ratios (Figure 26) is disconcerting in that the uncertainties in the assumed size distribution function are potentially as great as those in the rough experimental measurements. In an attempt to ascribe some reasonable degree of confidence to the calculated values, it seemed desirable to investigate the sensitivity of the theoretical computations to the form of the assumed distribution function. To this end, the extreme case of a mondisperse spray, in which all droplets have

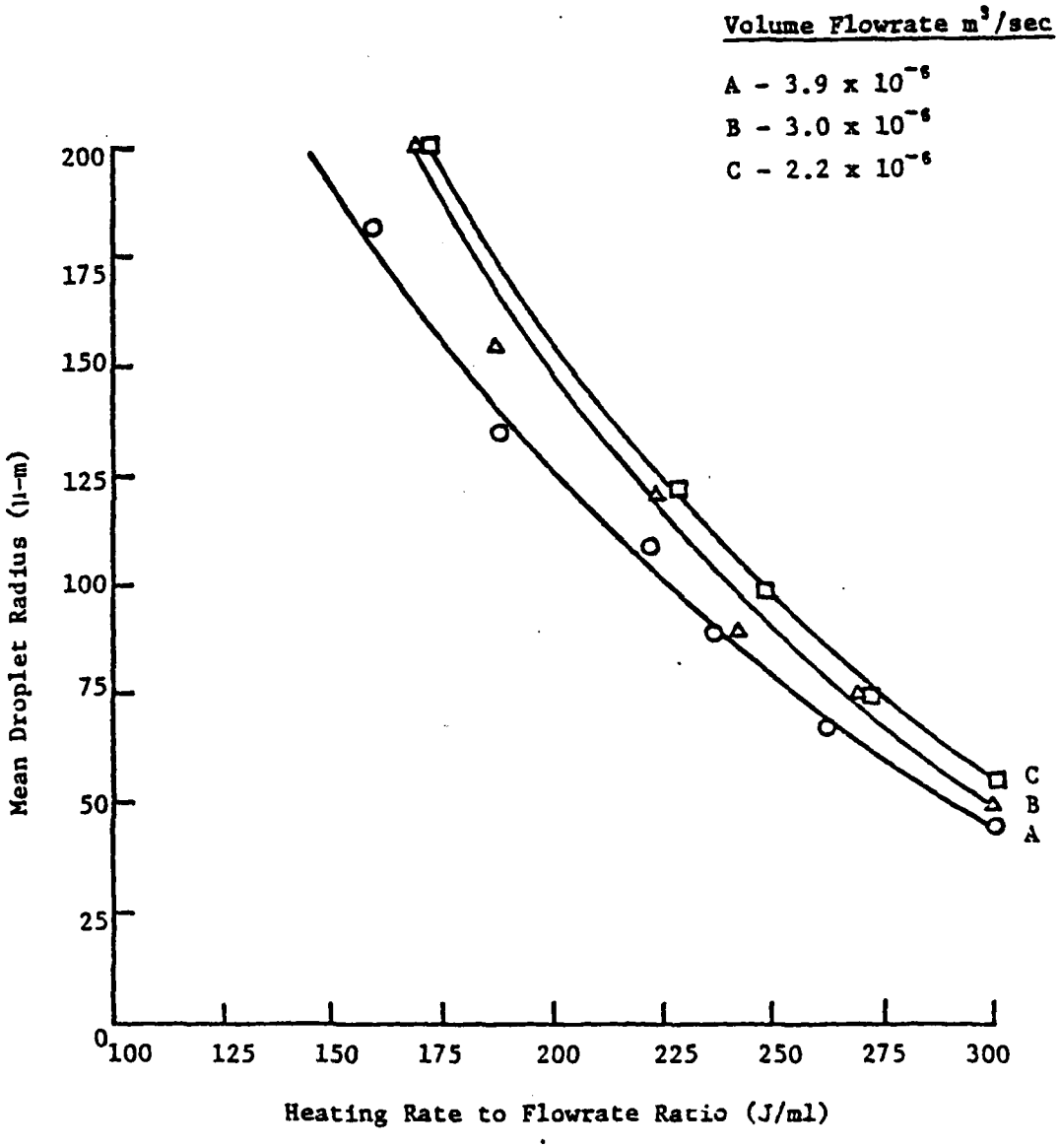

Figure 28. Mean Droplet Radius vs. Heating to Flowrate Ratio for Assumed Log-Normal Size Distribution

the same size, was applied to the experimental measurements of intensity ratio. The resulting variation of mean size with heating rate at each of the three flow rates is shown in Figure 29, and it is seen that both the shape and order of magnitude of the two sets of curves (Figures 28 and 29) are quite similar. In fact, the mean size range exhibits very little difference with assumed distribution function, except at the extreme ends of the heating rate-to-flowrate scale, where the monodisperse assumption produces more extreme values of the mean sizes.

As relative indicators of the spray behavior, however, the two results are in agreement, both showing the same favorable change in spray quality with increased heat addition and the somewhat less pronounced dependence of mean particle size upon pressure drop as evidenced by increasing flow rate. Based on this comparison between an admittedly limited selection of assumed size distributions, it appears that a simple function, such as the monodisperse case, is capable of providing as good a relative indication of spray performance as the more complicated continuous distribution. Thus it would appear that the time-consuming and potentially costly task of numerically integrating the attenuation index equation over the entire range of expected droplet radii may be sidestepped with acceptable levels of uncertainty.

Having established the laser attenuation experiment as a reasonable means of objectively detecting changes in the injector characteristics, we now turn our attention to determining how much, if any, physical significance (beyond the idea of a relative index of droplet size) can be attached to the "observed" droplet radius. Because the technique is based upon accepted theory and other arguments based on well-established

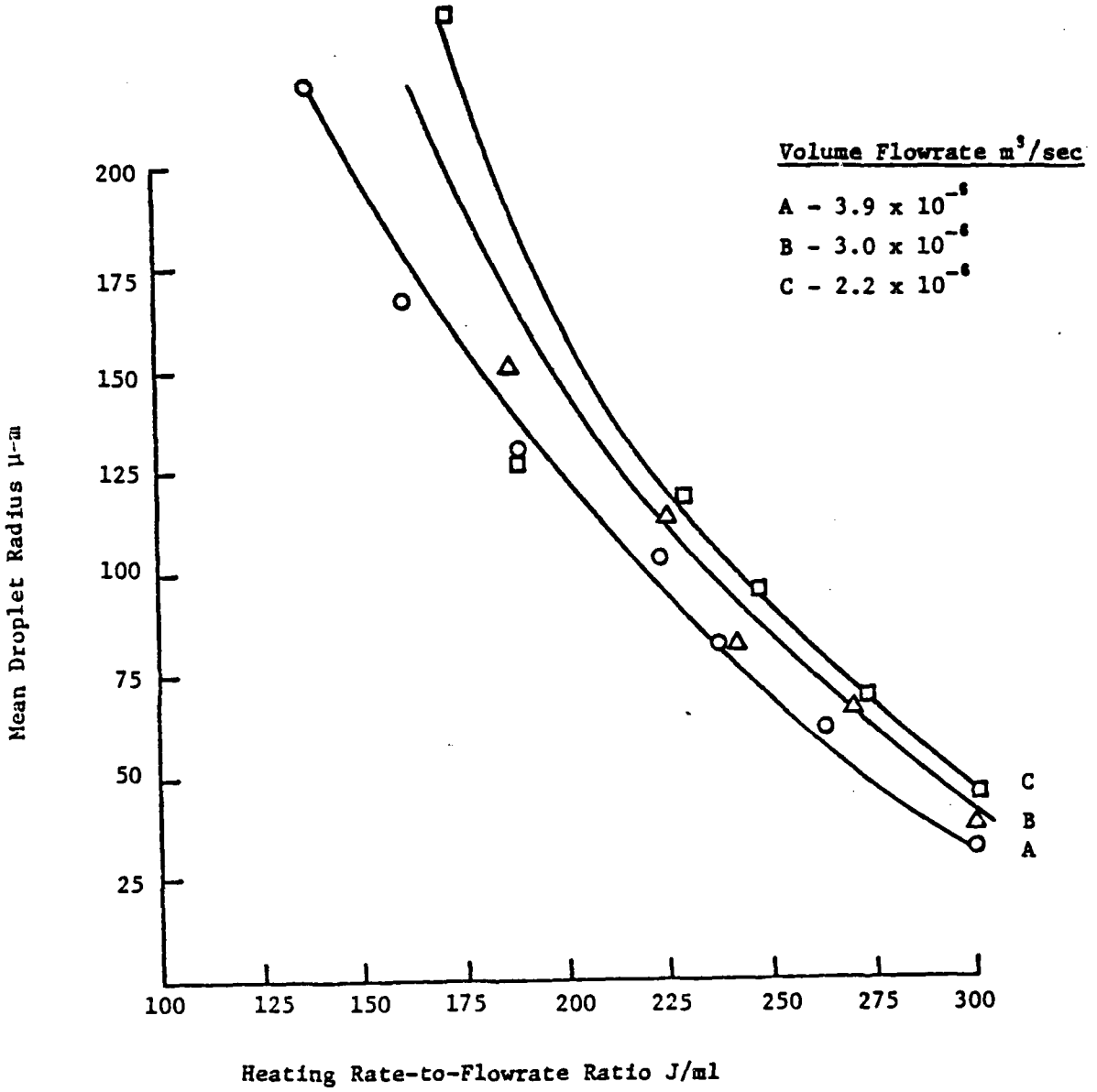

Figure 29. Mean Droplet Radius Vs. Heating to Flowrate Ratio For Assumed Monodisperse Size Distribution

physical principles, the question of attaching physical significance to the measured mean droplet radii is basically one of establishing the validity (or lack thereof) of the assumptions made in the interpretation of the experimental observations.

There is little one can say about the first assumption, that of discrete scatterers, other than simply to state it. However, if we consider the sizes "observed" in this study, we find the smallest value of about 30 μm much larger than typical molecular dimensions (< 10 Å). Furthermore, the evidence of the soot slide study clearly shows the presence of discrete droplets of fuel. Hence, the assumption of discrete scattering elements seems reasonable.

The second assumed condition for validity of the theory is that of single scattering of photons from the incident beam. A rule of thumb in popular use (Ref. 9) proposes that if the product of attenuation index and optical path length is less than 0.1, single scattering predominates. When the product is between 0.1 and 0.3, corrections for multiple scattering may be needed; while for values greater than 0.3, multiple scattering will dominate. In the experiments reported herein, this product varied from about 0.15 at the largest droplet sizes to nearly 1.5 for the smallest. This clearly suggests the presence of some multiple scattering, which may be examined from the point of view of its effect on the results at the small size end of the distribution spectrum. A careful comparison of the relative effects of this assumption on the calculated values indicates that agreement between experimental observations under conditions of multiple scattering with analytical solutions under assumed single scattering conditions is found for a mean

calculated droplet size larger than the actual size present in the spray. Thus, departure from the single scattering state will lead to predicted spray characteristics which are not as favorable as those likely to be encountered. To this end, the assumption is conservative when used in the evaluation of the Schladitz whisker injector.

The third assumed condition, that of spherical droplets, is satisfied if the influence of surface tension is much stronger than that of viscous drag on the particles. Selecting a drag coefficient dependent upon Reynolds number in the velocity range between approximately 10 meters/sec initial speed and 0.1 m/sec terminal speed, and noting the decrease of surface tension with increasing temperature, the sphericity criterion was calculated for a wide spectrum of particle sizes (30 - 200 μm). In all cases, it was found that surface tension effects predominate as the droplets approach terminal velocity. A further calculation of particle trajectories then showed that this steady-state velocity would be reached or approached to a satisfactory degree before entering the light-scattering region. The assumption of spherical particles is therefore justified.

SECTION V

CONCLUSIONS AND RECOMMENDATIONS

From the analysis of the test results obtained to date, several conclusions about the Schladitz Fuel Injector may be drawn:

1) With no pressure drop downstream from an injector, heat must be supplied in quantities sufficient to vaporize a significant proportion (33 to 71%) of the fuel flowing through the injector in order to attain a satisfactorily high performance rating (9.0 or 90% mist).

2) With a downstream pressure drop of 20 to 469 kPa, such as may be attained with a simple nozzle, a high performance rating (9.0) can be attained with a significantly lower heating rate, thereby vaporizing a smaller percentage of the fuel (0 to 17%) than without a pressure drop.

3) With or without a nozzle downstream from the injector, a maximum of 2% of the heat of combustion of the fuel must be returned to the fuel in the form of electrical energy to the injector. This includes any heat loss through the injector to the surroundings.

4) Collection of fuel spray droplets on soot-coated slides show that the mean replica size of particles leaving the injector and the fraction of large (greater than 100 μm) particle replica sizes decrease substantially with increased heating rate-to-flowrate ratio, and the fraction of small (less than 20 μm) particle replica sizes increases with increased heating rate-to-flowrate ratio.

5) Theoretically-based calculations of the dependency of mean particle size on heating rate-to-flowrate ratio, obtained from simple laser scattering experimental data, support the qualitative evidence of soot slide collection methods.

6) Although these semi-empirical results show wider divergence of mean sizes than the soot-slide experiments, their insensitivity to assumed distribution function is encouraging, and their validity in the present experimental circumstances is readily substantiated.

On the basis of the promising, but as yet preliminary and incomplete results, it is recommended that further tests be carried out on the Schladitz Fuel Injector to determine:

1) optimum or critical nozzle pressure drop for the best performance of the injector at a particular heating rate-to-flowrate ratio,

2) accurate particle size distribution using an appropriate optical technique applied over the anticipated range of mean sizes,

3) performance of this particular injector geometry using a different fuel type, e.g., a residual fuel oil,

4) actual combustion performance of the injector under realistic environmental conditions.

REFERENCES

1. J. B. Maxwell, Data Book on Hydrocarbons, D. VanNostrand Company, Inc., Princeton, N.J., 1960.

2. Baumuster, T., Avallone, E. A., and Baumster, III, T., Mark's Standards Handbook for Mechanical Engineers, McGraw-Hill Book Company, New York, 1978.

3. Barnett, H. C., and Hilbard, R. R., Properties of Aircraft Fuels, NACA TN 3276, Washington, August, 1956.

4. E. Giffen, A. Muraszew, The Atomization of Liquid Fuels, John Wiley and Sons, New York, 1953.

5. E. Sher, and C. Elata, Spray Formation from Pressure Cans by Flashing, Ind. Eng. Chem., Process Des. Dev., Vol. 16, No. 2, 1977 (page 237).

6. K. R. May, The Cascade Impactor: An Instrument for Sampling Coarse Aerosols, Journal of Sci. Insts., Vol. 22, Oct. 1945.

7. K. R. May, The Measurement of Airborne Droplets by the Magnesium Oxide Method, Journal of Sci. Insts., Vol. 27, May 1950.

8. Choi, S. C., Introductory Applied Statistics in Science, Prentice Hall, 1978.

9. van de Hulst, Light Scattering by Small Particles, Wiley, 1957.

APPENDIX A

PROPERTIES OF JET-A FUEL USED FOR THIS REPORT

Volume average boiling point = 409°F (209°C)

Weight average boiling point = 411°F (211°C)

Mean average boiling point = 410°F (210°C)

Molal average boiling point = 407°F (208°C)

Normal boiling point = 379°F (193°C)

Characterization Factor = 11.7

Molecular Weight = 163

Specific gravity, 60°F, 42°API or .8155

High heating value = 19,850 Btu/lbm

Low heating value = 18,550 Btu/lbm

Table 3

C. Ranges in the Test Results for Injectors 1 and 2

Injector Number	Volume Flowrate CC/SEC		Heating-to-Flowrate Ratio Joules/CC		Nozzle Pressure Drop Kilopascals		Injector Pressure Drop Kilopascals	
	Min.	Max.	Min.	Max.	Min.	Max.	Min.	Max.
1	2.41	6.49	0	491	0	--	52.8	355
1-1	2.43	7.55	0	582	0	448	267	905
2-1	.875	5.15	0	0	0	0	158	1,570
2-2	1.56	7.44	0	428	0	469	80.6	889
2-3	1.50	2.98	0	611	0	314	0	1,840

DISTRIBUTION LIST

Copy No.	
1 - 6	Power Programs (Code 473) Office of Naval Research 800 N. Quincy Street Arlington, VA 22217
7	Dr. David H. Lewis Jet Propulsion Lab 4800 Oak Grove Drive Mail Stop 122-101 Pasedena, CA 91103
8	Dr. Ronald Kostoff Department of Energy 400 First Street, N.W. Room 509 Washington, D.C. 20545
9 - 10	Mr. C. Richard Main Administrative Contracting Officer Office of Naval Research Resident Representative 2110 G. Street, N.W. Washington, D.C. 20037
11 - 12	J. E. Scott
13 - 14	G. B. Matthews
15	K. A. Havey, Jr.
16	J. Z. Colt, Jr.
17	M. A. Townsend
18	Office of Sponsored Programs
19 - 20	E. H. Pancake Clark Hall
21	RLES Files
22 - 82	See ONR Distribution List

D#200R

2269:LLL

Univ. of Virginia

Cntr. # N00014-77-C-0564
094-376

Schliditz Fuel Inj. Sys.

Recipient	No. of Copies
Defense Documentation Center Cameron Station Alexandria, Virginia 22314	(12)
Chief of Naval Research Department of the Navy Arlington, Virginia 22217 Attn: Mr. J.F. Patton, Jr., Code 473	(2)
Commander Naval Air Systems Command Department of the Navy Washington, D.C. 20360 Attn: Code 330 Code 310 Technical Library, Code 604	(1) (1) (1)
Commander Naval Sea Systems Command Department of the Navy CP# 6 Room 806 2211 Jefferson Davis Highway Arlington, Virginia 20360 Attn: Chas. L. Miller	(1)
The Boeing Company Headquarters Office P.O. Box 3707 Seattle, Washington 98124 Attn: Gas Turbine Division	(1)
General Electric Company Aircraft Gas Turbine Division Cincinnati, Ohio 45215 Attn: Manager of Engineering	(1)

Recipient	No. of Copies
Commanding Officer U.S. Army Research Office Box CM, Duke Station Durham, North Carolina 27706 Attn: Mr. Jas. Murray	(1)
Director National Aeronautics & Space Administration Headquarters Washington, D.C. 20546 Attn: Division Research Information	(1)
Director National Bureau of Standards Gaithersburg, Maryland 20760	(1)
Office of the Assistant Secretary of Defense (R&D) Room 3E1065- The Pentagon Washington, D.C. 20301 Attn: Technical Library	(1)
Aerojet-General Corporation P.O. Box 296 Azusa, California 91702 Attn: Librarian	(1)
AiResearch Manufacturing Company 9851 Sepulveda Boulevard Los Angeles, California 90045 Attn: Chief Engineer	(1)
General Motors Corporation Allison Division Indianapolis, Indiana 46206 Attn: Director of Engineering	(1)
General Electric Company Engineering Department Turbine Division Schenectady, New York 12305	(1)
General Electric Company Aircraft Turbine Department West Lynn, Massachusetts 01905	(1)
AVCO Corporation Lycoming Spencer Division 652 Oliver Street Williamsport, PA 17701	(1)

Recipient	No. of Copies
National Aeronautics & Space Administration Lewis Research Center 21000 Brookpark Road Cleveland, Ohio 44135	(2)
United Technologies Corporation Pratt & Whitney Aircraft Group East Hartford, Conn. 06118 Attn: Chief Engineer	(1)
Solar Aircraft Company San Diego, California 92101 Attn: Chief Engineer	(1)
United Technologies Research Center East Hartford, Conn. 06118 Attn: Director of Research	(1)
Commander Naval Surface Weapons Center White Oak Silver Spring, Maryland 20910 Attn: Library	(1)
Commander Naval Weapons Center China Lake, California 93555 Attn: Technical Library	(1)
Commander Wright Air Development Center Wright-Patterson Air Force Base, Ohio 45433 Attn: WCLPN-1, WCACD, WCLPS-1	(3)
Director U.S. Naval Research Laboratory 4555 Overlook Avenue, S.W. Washington, D.C. 20375 Attn: Technical Information Division	(6)
Office of Naval Research Department of the Navy Code 102D1 ARlington, Virginia 22217	(1)

Recipient	No. of Copies
Director Office of Naval Research Branch Office 536 South Clark Street Chicago, Illinois 60605	(1)
Officer in Charge Naval Ship Engineering Center Philadelphia Division Philadelphia, PA 19112	
Attn: Code 6700	(1)
Technical Library	(1)
Superintendent U.S. Naval Postgraduate School Monterey, California 93940	
Attn: Professor Max Platzer	(1)
Library, Code 0212	(1)
United Technologies Corporation Pratt & Whitney Aircraft Group Govt. Products Div. P.O. Box 2691 West Palm Beach, Florida 33402	(1)
Naval Ship Research & Development Center Annapolis Division Annapolis, Maryland 21402	
Attn: Library, Code A214	(1)
Director Ordnance Research Laboratory Pennsylvania State University University Park, PA 16802	(1)
Naval Surface Weapons Center Dahlgren, Virginia 22448	
Attn: Technical Library	(1)
Project SQUID Jet Propulsion Center School of Mechanical Engineering Purdue University Lafayette, Indiana 47907	
Attn: Professor Murthy	(1)

Recipient	No. of Copies
Director Applied Physics Laboratory 8621 Georgia Avenue Silver Spring, Maryland 20910 Attn: Library	(1)
Commander Air Force Aero Propulsion Laboratory Wright-Patterson Air Force Base Dayton, Ohio 45433	(1)
Commander Air Force Rocket Propulsion Laboratory Edwards Air Force Base, California 93523	(1)
Commander Air Force Office of Scientific Research 1400 Wilson Boulevard Arlington, Virginia 22209 Attn: B. Wolfson	(1)

UNIVERSITY OF VIRGINIA
School of Engineering and Applied Science

The University of Virginia's School of Engineering and Applied Science has an undergraduate enrollment of approximately 1,450 students with a graduate enrollment of approximately 500. There are 125 faculty members, a majority of whom conduct research in addition to teaching.

Research is an integral part of the educational program and interests parallel academic specialties. These range from the classical engineering departments of Chemical, Civil, Electrical, and Mechanical and Aerospace to departments of Biomedical Engineering, Engineering Science and Systems, Materials Science, Nuclear Engineering and Engineering Physics, and Applied Mathematics and Computer Science. In addition to these departments, there are interdepartmental groups in the areas of Automatic Controls and Applied Mechanics. All departments offer the doctorate; the Biomedical and Materials Science Departments grant only graduate degrees.

The School of Engineering and Applied Science is an integral part of the University (approximately 1,500 full-time faculty with a total enrollment of about 16,000 full-time students), which also has professional schools of Architecture, Law, Medicine, Commerce, Business Administration, and Education. In addition, the College of Arts and Sciences houses departments of Mathematics, Physics, Chemistry and others relevant to the engineering research program. This University community provides opportunities for interdisciplinary work in pursuit of the basic goals of education, research, and public service.